Journal of Medicinal Chemistry

Article

Antibacterial and Antibiofilm Activity of Cationic Small Molecules with Spatial Positioning of Hydrophobicity: An *In Vitro* and *In Vivo* Evaluation

Jiaul Hoque, Mohini Mohan Konai, Shanola Smitha Sequeira, Sandip Samaddar, and Jayanta Haldar

J. Med. Chem., **Just Accepted Manuscript** • DOI: 10.1021/acs.jmedchem.6b01435 • Publication Date (Web): 04 Nov 2016

Just Accepted

ACS Publications

Journal of Medicinal Chemistry is published by the American Chemical Society. 1155 Sixteenth Street N.W., Washington, DC 20036

Antibacterial and Antibiofilm Activity of Cationic Small Molecules with Spatial Positioning of Hydrophobicity: An *In Vitro* and *In Vivo* Evaluation

Jiaul Hoque, Mohini M. Konai, Shanola S. Sequeira, Sandip Samaddar and Jayanta Haldar*

Chemical Biology and Medicinal Chemistry Laboratory, New Chemistry Unit, Jawaharlal Nehru Centre for Advanced Scientific Research, Jakkur, Bengaluru 560064, India

ABSTRACT. More than 80% of the bacterial infections are associated with biofilm formation. To combat infections, amphiphilic small molecules have been developed as promising antibiofilm agents. However, cytotoxicity of such molecules still remains a major problem. Herein we demonstrate a concept in which antibacterial versus cytotoxic activities of cationic small molecules is tuned by spatial positioning of hydrophobic moieties while keeping positive charges constant. Compared to the molecules with more pendent hydrophobicity from positive centres (MIC = 1-4 μg/mL and HC_{50} = 60-65 μg/mL), molecules with more confined hydrophobicity between two centres show similar antibacterial activity but significantly less toxicity towards human erythrocytes (MIC = 1-4 μg/mL and HC_{50} = 805-1242 μg/mL). Notably, the optimized molecule is shown to be non-toxic towards human cells (HEK 293) at concentration it eradicates established bacterial biofilms. The molecule is also shown to eradicate preformed bacterial biofilm *in-vivo* in murine model of superficial skin infection.

INTRODUCTION

It is estimated that more than 80% of bacterial infections are accompanied by the biofilm formation.[1] Biofilms that form on biotic surfaces, e.g., mammalian tissue, are associated with a vast number of bacterial infections such as chronic lung infections in cystic fibrosis patients, periodontitis, endocarditis, skin infections, etc.[2,3] Moreover, bacterial biofilms play significant role in many nosocomial infections due to colonization on abiotic surfaces such as catheters and other medical devices.[4,5] In order to prevent infections associated with bacterial biofilms, various synthetic antibiofilm agents capable of inhibiting biofilm formation have been developed.[6-13] Nonetheless, from a clinical standpoint, infections caused by already established biofilms pose significant threat to human health as biofilms are inherently resistant to host immune system and conventional therapeutic antibiotics.[14-16] It is therefore necessary to develop molecules that are capable of eradicating preformed bacterial biofilms while sparing the mammalian cells.

As the biofilms are covered by anionic exopolymeric substances (EPS) composed of mostly polysaccharide, proteins and extracellular negatively charged DNA, cationic small molecules are known to interact with the biofilm matrix thereby disrupts the matrix.[17-22] Further, small molecules have also been shown to destroy the matrix-embedded bacteria which are difficult to kill otherwise thereby leading to eradication of established biofilm.[23-27] Interestingly, some of the molecules were shown to have the abilities of both inhibiting bacterial biofilm formation and eradicating established biofilms.[28-31] However, identification of small molecules that eradicate biofilm and kill encased bacteria without affecting the mammalian cell viability still remains a major challenge. In general antibacterial activity versus cytotoxicity of amphiphilic small molecules has been tuned by varying length of the hydrophobic chain, the number of positive charges and the hydrophobic/hydrophilic balance of the molecules.[32-42] Importantly, the role of positive charges and thereby tuning the

amphiphilic balance were effectively shown to improve the antibacterial activity while minimising the toxicity of cationic small molecules.[43-46] It has also been observed that the choice of scaffold and hence spacing of positive charges improves the selectivity of the molecules.[43-46] However, how the activity and toxicity of an amphiphilic small molecule varies as a function of spatial positioning of the hydrophobic moieties while keeping the positive charges unchanged remains largely unexplored. For instance, how the activity and toxicity of a small molecule bearing two positive charges differ when the hydrophobic moieties are more confined between two positive centres as opposed to being pendent from the positive centres. It is well known that optimum amphiphilicity is an essential criterion to achieve antibacterial activity; however increase in hydrophobic character for improving antibacterial activity is also known to increase cytotoxicity. Herein we hypothesized that cytotoxicity of the molecules could further be tuned by spatial positioning of hydrophobic moiety in molecules with optimum amphiphilicity.

Interestingly, spatial controlling of hydrophobicity was shown to significantly affect the toxicity of cationic small molecules with negligible changes in antibacterial activity. Confining hydrophobic moiety more between two positive centres of a small molecule remarkably reduced its toxicity towards mammalian cells compared to a molecule with less confined hydrophobicity (Figure 1). In a model lipid-small molecule interaction studies, it was observed that molecules with more confined hydrophobicity interacted selectively with negatively charged lipid membrane of bacteria whereas molecules with more pendent hydrophobicity interacted with both negatively charged lipid membrane of bacteria and zwitterionic lipid membrane of mammalian cells. Moreover, the optimised molecule showed excellent efficacy in eradicating established bacterial biofilms *in-vitro*. While the lack of ability to eradicate established bacterial biofilms under complex *in-vivo* conditions has been a major setback for antibiofilm agents to be translated into clinics, we also show that the

optimized molecule is capable of annihilating preformed methicillin-resistant *Staphylococcus aureus* (MRSA) biofilms in murine model. The above facts therefore indicated that the study might hold promise in designing and developing safe and potent biofilm disruptors.

RESULTS AND DISCUSSION

Design and Synthesis of Small Molecules. To establish the above facts, we synthesized two series of cationic small molecules (**1a-3a** and **1b-3b**) that differ only in spatial positioning of hydrophobicity (**1a** (n = 2; R = $–C_{10}H_{21}$), **1b** (n = 4; R = $–C_{10}H_{21}$), **2a** (n = 6; R = $–C_8H_{17}$), **2b** (n = 8; R = $–C_8H_{17}$), **3a** (n = 10; R = $–C_6H_{13}$) and **3b** (n = 12; R = $–C_6H_{21}$)) (Figure 1). In each series the number of methylene groups was gradually increased between the positive centers of the molecules with the gradual decrease in the number of methylene groups in pendent alkyl chains (Figure 1a to 1b to 1c). Two series of molecules with a total of 22 and 24 carbon atoms in their pendent and confined alkyl chains were synthesized (the number includes only the carbon atoms present in the alkyl chains except the common positive charges and amide bonds) (Figure 1). Molecules **1a** and **1b** possess the maximum pendent hydrophobicity (Figure 1a), **2a** and **2b** possess middling pendent hydrophobicity with moderately confined hydrophobic chain (Figure 1b) whereas **3a** and **3b** possess the least pendent hydrophobicity with mostly confined hydrophobic chain (Figure 1c). We deliberately avoided using very low pendent alkyl chain, as the molecules with such chains did not yield reasonable antibacterial activity. All the small molecules were found to be soluble in water. However, solubility of the molecules with more confined hydrophobicity (**3a** and **3b**) was less compared to the molecules with pendent or moderately confined hydrophobicity (**1a, 1b, 2a** and **-2b**).

The molecules were synthesized in a simple three step method (Scheme 1).[32] First, *N,N,N′,N′*-tetramethyl-α,ω-diaminoalkanes were synthesized from α,ω-dibromoalkanes by

reacting the bromoalkanes with *N,N*-dimethylamine. The length of the hydrocarbon chain in α,ω-dibromoalkanes was varied accordingly to obtain molecules with more confined or more pendent hydrophobicity (Scheme 1). Second, *N*-alkyl-1-bromoethanamide with different prefixed chain lengths was synthesized by reacting alkylamines with bromoacetyl bromide. Finally, *N,N,N′,N′*-tetramethyl-α,ω-diaminoalkanes were reacted with *N*-alkyl-1-bromoethanamide to obtain the cationic small molecules (Scheme 1). The molecules were characterized by FT-IR, ^{1}H NMR, ^{13}C NMR and high resolution mass spectrometry (HRMS). These molecules bear structural resemblance with antimicrobial peptides (AMPs) that are known to interact with the bacterial cell membrane in a non-specific manner which make them less susceptible towards microbial resistance development. However, while the usage of AMPs is limited due to their proteolytic susceptibility, high production cost and high toxicity, easily synthesizable, non-toxic cationic small molecules with non-peptidic amide bonds and spatially tuned hydrophobicity would be helpful. Recently other than expected electrostatic and hydrophobic interactions, amphiphilic antimicrobials with amide groups have been shown to interact with bacterial cell membrane via hydrogen bonding thereby leading to enhanced activity.[47] In addition to the spatial control of hydrophobicity, we also studied the role of increasing hydrophobicity on biological activity profile of the small molecules. A total of 12 more cationic small molecules were synthesized by varying confined alkyl chain length while keeping the pendent chain length constant (**1c-1f**; **2c-2f** and **3c-3f**; Scheme 1). Thus a total of 18 compounds were synthesized and studied (**1c** (n = 6; R = $-C_{10}H_{21}$), **1d** (n = 8; R = $-C_{10}H_{21}$), **1e** (n = 10; R = $-C_{10}H_{21}$) and **1f** (n = 12; R = $-C_{10}H_{21}$); **2c** (n = 2; R = $-C_8H_{17}$), **2d** (n = 4; R = $-C_8H_{17}$), **2e** (n = 10; R = $-C_8H_{17}$) and **2f** (n = 12; R = $-C_8H_{17}$), and **3c** (n = 2; R = $-C_6H_{13}$), **3d** (n = 4; R = $-C_6H_{13}$), **3e** (n = 6; R = $-C_6H_{13}$), **3f** (n = 8; R = $-C_6H_{13}$). The details of characterization and spectral data were provided in the experimental section and in the Supporting Information (Figure S1-S18, Supporting Information). The purity of the

molecules was tested by HPLC and was found to be more than 95% (Figure S19, Supporting Information).

Antibacterial and Hemolytic Activities. Each compound was first tested for its antibacterial activity against Gram-positive *S. aureus* and Gram-negative *E. coli*. The activity was represented in terms of minimum inhibitory concentration (MIC) and defined as the minimum concentration required to inhibit bacterial growth.[48] Notably MIC of the molecules within a series (**1a-3a** or **1b-3b**) were found to be similar thus indicating that the spatial positioning of hydrophobicity did not alter their antibacterial efficacy (Figure 2). For example, MIC values of **1b**, **2b** and **3b** were found to be 1-2 μg/mL against *S. aureus* and 2 μg/mL each against *E. coli* respectively (Figure 2a). However, when tested against human erythrocytes, hemolytic activity (represented as HC_{50}, concentration at which 50% hemolysis occurs) of the molecules within a series was found to vary remarkably. For example, HC_{50} values of **1b**, **2b** and **3b** were found to be 60 μg/mL, 212 μg/mL and 805 μg/mL respectively. The above results thus indicated that the molecule with confined hydrophobicity (**3b**) was more selective towards bacteria over human erythrocytes than the molecules with pendent hydrophobicity (**1b** and **2b**). To compare the potency of the molecules, selectivity (S = HC_{50}/MIC) which is one of the measures of therapeutic efficacy was calculated. Selectivity of the molecules **1b**, **2b** and **3b** were 30, 182 and 805 against *S. aureus* and 30, 106 and 402 against *E. coli* respectively (Figure 2b). Thus the above results indicated that the **3b** with more confined hydrophobicity are most selective. Similar trends of antibacterial and hemolytic activities were observed for the other series (series 1). MIC values of **1a**, **2a** and **3a** were found to be 2-4 μg/mL against *S. aureus* and 4-6 μg/mL against *E. coli* respectively whereas HC_{50} values were found to be 65 μg/mL, 300 μg/mL and 1242 μg/mL respectively (Figure 2a). Consecutively, selectivity of **1a**, **2a** and **3a** were 32, 150 and 310 towards *S. aureus* and 16, 50 and 207 towards *E. coli* respectively (Figure 2b). The above results thus

demonstrated the versatility of the concept. Notably, when tested against methicillin-resistant *S. aureus* (MRSA), similar results were observed against MRSA for both the series (Table 1). The optimised molecule **3b** showed MIC value of 2 μg/mL against MRSA thereby making it a promising antibacterial agent.

Interestingly, when the hydrophobic character hence the overall amphiphilic balance of the molecules was varied mainly by varying the confined alkyl chain while keeping the pendent alkyl chain constant (**1a-1f** or **2a-2f** or **3a-3f**); both antibacterial and hemolytic activities were found to vary differently depending on the length of both pendent and confined alkyl chains. For example, when the length of confined chain was increased for the molecules with $-C_{10}H_{21}$ pendent chain, antibacterial activity and hemolytic toxicity of the molecules were found to vary non-significantly except molecule **1f** (Table 1). For example, MIC values of molecules **1a-1e** were 2-4 μg/mL against *S. aureus* and 2-8 μg/mL against *E. coli* respectively. However, HC_{50} values of molecules were found to be 50-65 μg/mL against hRBC (Table 1). The low activity of **6a** (MIC values were 31 μg/mL against *S. aureus* and 500 μg/mL against *E. coli* respectively) could be due to its very high hydrophobic character which might lead to aggregation of the molecules in tested media. On the other hand, when length of the confined chain was increased for the molecules with $-C_8H_{17}$ pendent chain, antibacterial activity was found to vary slightly while toxicity towards human erythrocytes varied greatly (Table 1). For example, MIC values of molecules **2a-2f** were 1-2 μg/mL against *S. aureus* and 1-8 μg/mL against *E. coli* respectively. Whereas HC_{50} values of these molecules were found to be 50-350 μg/mL against hRBC (Table 1). Notably, when the length of confined chain was increased for the molecules with $-C_6H_{13}$ pendent chain, antibacterial activity was found to vary significantly while toxicity towards human erythrocytes remained almost unchanged (Table 1). For example, MIC values of molecules **3a-3f** were 1-125 μg/mL

against *S. aureus* and 2-250 μg/mL against *E. coli* respectively. Whereas HC_{50} values of the molecules were found to be close to or greater than 1000 μg/mL against hRBC (Table 1). The results are therefore in good agreement with the earlier reports.[29] In summary, above facts indicated that confining hydrophobicity in molecules with optimized amphiphilic balance is important to obtain active yet non-toxic compounds.

To strengthen the non-cytotoxic behaviour of the molecules with confined hydrophobicity, human embryonic kidney (HEK 293) cells were treated with **1b**, **2b** and **3b**, all at 32 μg/mL and were imaged by fluorescence microscopy using membrane permeable green fluorescent dye calcein-AM and membrane impermeable red fluorescent dye propidium iodide (PI).[20] While the untreated cells showed complete green fluorescence (Figure 3a), cells treated with molecule **1b** showed complete red fluorescence at the tested concentration indicative of cell death (Figure 3b). Cells treated with molecule **2b** displayed partially green fluorescence thereby indicating the presence of some live cells (Figure 3c). Interestingly, cells treated with molecules **3b** showed complete green fluorescence at the same concentration thus indicating the survival of kidney cells (Figure 3d). It should be mentioned that the molecules showed similar activity against HEK cells when treated at a lower concentration (at 16 μg/mL) and at a higher concentration (at 64 μg/mL). When the cells were treated at 16 μg/mL, **3b** treated cells showed complete green fluorescence with higher cell density in contrast to the cells treated with **1b** and **2b** which also showed green fluorescence but with lesser cell density (Figure S20, Supporting Information). When the cells treated at 64 μg/mL, **3b** treated cells still showed mostly green fluorescence in sharp contrast to the cells treated with **1b** and **2b** at the same concentration which showed completely red fluorescence (Figure S21, Supporting Information). The above facts thereby indicated the lower cytotoxic nature of **3b** compared to molecules with less confined hydrophobicity (**1b** and **2b**).

Effect on Membrane Fluidity and Membrane Permeabilization. We speculated that the molecules with less confined hydrophobicity would interact more strongly with both anionic bacterial cell membrane as well as zwitterionic mammalian cell membrane because of more flexible pendent alkyl chain.[49] Hence we studied the interaction of these molecules with both bacterial and mammalian cell membranes using model lipid bilayers. Liposomes were made using anionic DPPG and zwitterionic DPPE (DPPG:DPPE = 88:12) mimicking the bacterial cell membrane, and zwitterionic DPPC mimicking the red blood cell membrane with a hydrophobic dye Laurdan (6-Dodecanoyl-2-dimethylamino-naphthalene).[47] In phospholipid liposomes, the dye is known to get located closer to the hydrated aqueous surface of liposomes and sense freely rotating water molecules. Upon interaction with the cationic lipophilic molecules, disorder of lipid molecules in the membrane allows penetration of more water molecules into the bilayer leading to more hydration of the membrane surface. The extent of hydrataion is commonly quantified by determining the general polarization (GP = $(I_{440}-I_{490})/(I_{440}+I_{490})$ where I is the fluorescence intensity at 440 nm and 490 nm for an excitation at 350 nm. In general, lower the GP, higher is the membrane disorder.[50,51] Interestingly, GP for both **1b** and **3b** treated liposomes was found to be lower compared to the untreated DPPG:DPPE liposome at all three concentrations tested (25 μg/mL, 50 μg/mL and 100 μg/mL) (Figure 4a). These results suggested that both **1b** and **3b** were effective in disordering anionic DPPG:DPPE bilayer to the similar extent. However, against DPPC liposomes, **1b** showed large reduction in GP than **3b** when compared to the untreated bilayer (Figure 4b). These results thus indicated that the molecule with less pendent hydrophobicity interacted to a much lesser extent with the zwitterionic mammalian cell membrane.

To confirm that the cationic small molecules act by disrupting the bacterial cell membrane integrity, molecular mechanism of action was studied using spectroscopic methods against both Gram-positive and Gram-negative bacteria. To establish whether the

molecules act by depolarizing the cell membrane of bacteria, 3, 3'-dipropylthiadicarbocyanine iodide ($DiSC_3 5$), a membrane-potential sensitive dye, was used.[52] In general, the dye is taken up by the bacteria due to the potential gradient and accumulation in the membrane leads to a decrease in its fluorescence intensity because of self-quenching. When the membrane-potential is lost, the dye would be displaced into the solution thus would lead to an enhancement in fluorescence intensity. Notably, upon treating bacteria with the molecules, fluorescence intensity of $DiSC_3 5$ was found to increase for both *S. aureus* and *E. coli* (Figure 5a and 5b). The above fact therefore indicated that the molecules dissipated membrane-potential of both Gram-positive and Gram-negative bacteria. The ability of the small molecules to permeabilize the cell membrane of bacteria was further studied using a cell membrane impermeable dye propidium iodide (PI).[53] Once the cell-membrane of bacteria is compromised, PI is known to enter inside bacteria and fluoresce upon intercalating to the cellular DNA. Notably, when bacteria were treated with the molecules, fluorescence intensity of PI was found to increase against both *S. aureus* and *E. coli* (Figure 5c and 5d). Thus the molecules were also shown to be efficient in permeabilizing the cell membranes of bacteria. In summary, the above studies indicated that the cationic small molecules indeed interacted with the negatively charged cell membrane of bacteria and disrupted the membrane integrity.

Biofilm Disrupting Ability. Next we tested the ability of the optimized molecule to eradicate established bacterial biofilms. *S. aureus* and *E. coli* biofilms were treated with **3b** (at 32 μg/mL) and analyzed for cell counting as well as observed by confocal laser scanning microscopy (CLSM).[54] Molecule **3b** was found to reduce 9.2 log bacterial burden against *S. aureus* biofilm and 7.1 log against *E. coli* biofilm respectively thus showing the ability to destroy biofilm-encased bacteria. The biofilm disrupting property of the molecule was further established by CLSM via staining with green fluorescent dye SYTO 9. In the untreated samples, thick and matured biofilms of thickness ~14-18 μm were seen (Figure 6a and 6c)

while treated samples showed scattered mono layered bacteria of only 2-3 μm thickness against both *S. aureus* and *E. coli* respectively (Figure 6b and 6d). These results further demonstrated the ability of the molecules to eradicate establish bacterial biofilms at a concentration at which it did not cause any cytotoxic effect. We also determined the minimum biofilm eradication concentration (MBEC) for the cationic molecules. MBEC values of **1b** and **3b** were found to be 31.2-62.5 μg/mL against *S. aureus* and 62.5-125 μg/mL against *E. coli* respectively (Table S1). The above results thus indicated that these molecules are capable of annihilating established biofilms completely. To evaluate the potential of these small molecules as antibiofilm agents, MBEC values were also compared with some common antiseptics (BAC-14 and DDAC-10) and cationic amphiphiles (DTAB and CTAB). Notably, the molecules showed similar or even better MBEC values compared to those of commercial quaternary compounds (Table S1).

***In-vivo* Toxicity and Antibiofilm Activity.** *In-vivo* toxicity of the cationic small molecules still remains a major concern for the molecules to be used in healthcare applications.[55] Thus we briefly evaluated the toxic effect of the optimized molecule (**3b**) by determining the lethal dose (LD_{50}) upon topical application in mice. LD_{50} values for both **1b** and **3b** were found to be more than 200 mg/kg in an acute dermal toxicity study (OECD 425). However, no visible inflammation or abnormal skin reaction was observed for **3b** at 200 mg/kg. On the other hand, **1b** showed high on-set toxicity as darkening of the skin and relatively much lesser fur appearance were observed after 14 days of post-treatment. Another important limitation of the antimicrobials is their relatively poor potency under *in-vivo* conditions. In general, it has been observed that small molecules lack the ability to eliminate preformed bacterial biofilms *in-vivo*, which has largely limited their pre-clinical entry.[55] Herein we studied *in-vivo* efficacy of the most potent molecule to eradicate preformed biofilm of MRSA-one of the leading biofilm forming and the most common bacteria that causes many nosocomial infections.

Importantly, the optimised molecule showed remarkable biofilm eradicating ability under *in-vivo* conditions. In a murine model of superficial skin infection and biofilm formation, a wound was first induced on the back of mice (dorsal midline) and then infected with MRSA.[56] The biofilms formed after 24 h of infection were then treated by **3b** topically (40 mg/kg once a day) (Figure 7a) for four days. After 18 h of the application of last dosage, mice were sacrificed and skin tissues were collected. Notably, **3b** treated skin tissue samples showed 5.3 log (> 99.999%) reduction of MRSA compared to the untreated tissue samples (p value <0.0001). In contrast, fusidic acid and silver nanoparticle containing commercial ointment (ReliHeal) which are used in clinics to treat skin infections, were found to reduce MRSA count by 2.2 and 2.3 log reduction at 40 mg/kg and 200 mg/kg respectively (Figure 7b) (p values were 0.0183 and 0.0025 respectively). The fact that the molecule **3b** was much more effective in comparison to the approved drug fusidic acid emphasizes on the clinical potential of the molecule. The ability of the small molecule in eradicating matured biofilm under *in-vivo* conditions was further established by imaging skin tissue samples with scanning electron microscopy. Tissue samples after 24 h of infection showed the presence of a thick dense MRSA layer thereby indicated the formation and persistence of biofilm (Figure 7c). The treated skin tissue sample, on the other hand, showed negligible number of bacteria on the tissue surface (Figure 7d). These result thus indicated the ability of the optimised molecule to eradicate bacterial biofilms under *in-vivo* conditions.

CONCLUSION

In summary, we demonstrated a concept of developing non-toxic small molecular biofilm disruptors by spatial positioning of the hydrophobicity. Molecules with more pendent hydrophobicity showed higher membrane disrupting ability, as indicated by their high antibacterial as well as cytotoxic activities. Molecules, on the other hand, with more confined

hydrophobicity showed higher antibacterial but significantly lower cytotoxic activities. Using model lipid bilayers and spectroscopic methods, the cationic molecules were shown to depolarize and permeabilize the bacterial cell membrane thereby leading to cell inactivation. Importantly, the optimized molecule was found to be non-toxic towards mammalian cells at a concentration at which it eradicated established bacterial biofilms. Moreover, the molecule was also found to eradicate preformed bacterial biofilm under more complex *in-vivo* conditions without causing substantial skin toxicity. The results furnished herein thus emphasize the potential of this class of molecules to be useful in guiding and developing future antibacterial and antibiofilm small molecules with improved biocompatibility.

EXPERIMENTAL SECTION

1. Materials and Instrumentation. 1-Aminohexane, 1-aminooctane, 1-aminodecane, bromoacetyl bromide, *N,N,N′,N′*-tetramethyl-1,2-diaminoethane, *N,N,N′,N′*-tetramethyl-1,4-diaminobutane, 1,6-dibromohexane, 1,8-dibromooctane, 1,10-dibromodecane and 1,12-dibromododecane were purchased from Sigma-Aldrich and used as received. Anhydrous potassium carbonate (K_2CO_3), anhydrous sodium sulphate (Na_2SO_4), phosphorous pentaoxide (P_2O_5), dichloromethane, chloroform, acetonitrile and anhydrous diethylether were purchased from SD Fine, India and were of analytical grade. Dichloromethane, chloroform and acetonitrile were dried over P_2O_5 and stored over activated molecular sieves (4 Å). Nuclear magnetic resonance (NMR) spectra were recorded using Bruker AMX-400 (400 MHz for ^{1}H NMR and 100 MHz for ^{13}C NMR) spectrometer in suitable deuterated solvents. High resolution mass spectra were recorded on a 6538-UHD Accurate mass Q-TOF LC-MS high resolution mass-spectrometer (HRMS). Fourier transform infrared (FT-IR) spectra were recorded on an attenuated total reflectance (ATR) FT-IR spectrometer using diamond crystal as ATR crystal. The purity (>95%) of the small molecules was determined by HPLC. For

optical density and fluorescence measurements, Tecan Infinite Pro series M200 microplate reader was used. *Staphylococcus aureus* (MTCC 737) and *Escherichia coli* (MTCC 443) were obtained from MTCC (Chandigarh, India). Methicillin-resistant *Staphylococcus aureus* (MRSA) (ATCC 33591), were purchased from ATCC (Rockville, MD, USA). Bacterial growth media and agar were supplied by HIMEDIA, India. Studies on human subjects such as human red blood cells (hRBC) and human embryo kidney cells (HEK 293) were performed according to the guidelines approved by Institutional Bio-Safety Committee (IBSC) at Jawaharlal Nehru Centre for Advanced Scientific Research (JNCASR). Studies on animals were performed in accordance with protocols approved by the Institutional Animal Ethics Committee (IAEC) at the Jawaharlal Nehru Centre for Advanced Scientific Research (JNCASR).

2. Synthesis of Small Molecules

2. 1. General Synthesis of N,N,N′,N′-Tetramethyl-α,ω-diaminoalkanes. N,N,N′,N′-tetramethyl-α,ω-diaminoalkanes were synthesized with the slight modifications following an earlier report.[32] Briefly, $NHMe_2$ gas was collected into dry $CHCl_3$ (40 mL) in a screw-top pressure tube set at 0 $^{\circ}$C until the volume of the resulting solution became 1.5 fold (~60 mL). Dibromoalkane (10 g) was then added through syringe and stirred for 24 h at room temperature. After cooling, the reaction mixture was transferred into a round bottomed flask quantitatively. Excess gas was removed by heating the reaction mixture slowly. Finally, the mixture was diluted with $CHCl_3$ followed by washing with NaOH (2 M, 100 mL × 2) solution. Organic layer was then collected and passed through anhydrous Na_2SO_4. Finally, the organic solution was dried and light yellow gummy liquid was obtained as product with quantitative yield.

N,N,N′,N′-Tetramethyl-1,6-diaminohexane: ^{1}H NMR (400 MHz, $CDCl_3$): δ 1.288-1.342 (m, $-CH_2CH_2CH_2NMe_2$, 4H), 1.421-1.476 (m, $-CH_2CH_2CH_2NMe_2$, 4H), 2.204-2.255 (br. m,

–CH_2CH_2N*(*CH_3*)*$_2$ and –CH_2CH_2*CH_2*NMe_2, 16H); ^{13}C NMR (100 MHz, $CDCl_3$): δ 27.636, 27.879, 45.656, 60.030.

N,N,N′,N′-Tetramethyl-1,8-diaminooctane: ^{1}H NMR (400 MHz, $CDCl_3$): δ 1.223-1.314 (br. m, –*(*CH_2*)*$_2$$CH_2CH_2NMe_2$, 8H), 1.398-1.451 (m, –$(CH_2)_2$*$CH_2$*$CH_2NMe_2$, 4H), 2.179-2.228 (br. m, –CH_2CH_2N*(*CH_3*)*$_2$ and –$(CH_2)_2CH_2$*CH_2*NMe_2, 16H); ^{13}C NMR (100 MHz, $CDCl_3$): δ 27.615, 27.877, 29.685, 45.638, 60.092.

N,N,N′,N′-Tetramethyl-1,10-diaminodecane: ^{1}H NMR (400 MHz, $CDCl_3$): δ 1.257 (br. m, –*(*CH_2*)*$_3$$CH_2CH_2NMe_2$, 12H), 1.409-1.444 (m, –$(CH_2)_3$*CH_2*CH_2NMe_2, 4H), 2.192-2.242 (br. m, –CH_2CH_2N*(*CH_3*)*$_2$ and –$(CH_2)_3CH_2$*CH_2*NMe_2, 16H); ^{13}C NMR (100 MHz, $CDCl_3$): δ 27.671, 27.908, 29.703, 29.753, 45.643, 60.119.

N,N,N′,N′-Tetramethyl-1,12-diaminododecane: ^{1}H NMR (400 MHz, $CDCl_3$): δ 1.246-1.262 (br. m, –*(*CH_2*)*$_4$$CH_2CH_2NMe_2$, 16H), 1.410-1.445 (m, –$(CH_2)_4$*CH_2*CH_2NMe_2, 4H), 2.190-2.231 (br. m, –CH_2CH_2N*(*CH_3*)*$_2$ and –$(CH_2)_4CH_2$*CH_2*NMe_2 and, 16H); ^{13}C NMR (100 MHz, $CDCl_3$): δ 27.682, 27.922, 29.753, 29.775, 45.652, 60.130.

2.2. Synthesis of N-Alkyl-1-bromoethanamide. 1-Aminoalkanes (60 mmol) was dissolved in CH_2Cl_2 (200 mL). K_2CO_3 (90 mmol) was dissolved in water (150 mL) and the aqueous solution was then added to the organic solution. The two phase solution was cooled to 4-5 °C. Bromoacetyl bromide (90 mmol) in CH_2Cl_2 (50 mL) was added drop wise to the solution while maintaining temperature at 4-5 °C for about 30 min. The reaction mixture was then set at room temperature and stirred for about 4 h. After the reaction organic layer was collected and the aqueous solution was washed with CH_2Cl_2 (3 × 50 mL). Organic solution was then washed with water (3 × 100 mL), passed over the anhydrous Na_2SO_4 and concentrated to give product with quantitative yields.

N-Hexyl-1-bromoethanamide: FT-IR: 3255 cm^{-1} (amide NH str.), 2935 cm^{-1} (CH_2 assym. str.), 2852 (CH_2 sym. str.), 1678 cm^{-1} (amide I, C=O str.), 1555 cm^{-1} (amide II, NH ben.),

1468 cm^{-1} (CH_2 scissor); ^1H NMR: (400 MHz, $CDCl_3$): δ 0.880 (t, terminal –*CH₃*, 3H), 1.325 (m, $-CH_2(CH_2)_3CH_3$, 6H), 1.539 (m, $-CH_2(CH_2)_3CH_3$, 2H), 3.277 (m, –CONH*CH₂*–, 2H), 3.884 (s, –CO*CH₂*Br, 2H), 6.468 (br. s, amide –*NH*CO, 1H); ^{13}C NMR (100 MHz, $CDCl_3$): δ 14.111, 22.643, 26.601, 29.357, 29.534, 31.531, 40.411, 165.335.

N-Octyl-1-bromoethanamide: FT-IR: 3258 cm^{-1} (amide NH str.), 2943 cm^{-1} (CH_2 assym. str.), 2857 (CH_2 sym. str.), 1671 cm^{-1} (amide I, C=O str.), 1561 cm^{-1} (amide II, NH ben.), 1460 cm^{-1} (CH_2 scissor); ^1H NMR: (400 MHz, $CDCl_3$): δ 0.882 (t, terminal –*CH₃*, 3H), 1.290 (m, $-CH_2(CH_2)_5CH_3$, 10H), 1.521 (m, $-CH_2(CH_2)_5CH_3$, 2H), 3.275 (m, –CONH*CH₂*–, 2H), 3.884 (s, –CO*CH₂*Br, 2H), 6.462 (br. s, amide –*NH*CO, 1H); ^{13}C NMR (100 MHz, $CDCl_3$): δ 14.214, 22.765, 26.947, 29.293, 29.325, 29.401, 29.548, 31.901, 40.425, 165.326.

N-Decyl-1-bromoethanamide: FT-IR: 3254 cm^{-1} (amide NH str.), 2928 cm^{-1} (CH_2 assym. str.), 2855 (CH_2 sym. str.), 1678 cm^{-1} (amide I, C=O str.), 1555 cm^{-1} (amide II, NH ben.), 1472 cm^{-1} (CH_2 scissor). ^1H NMR: (400 MHz, $CDCl_3$): δ 0.880 (t, terminal –*CH₃*, 3H), 1.263-1.304 (m, $-CH_2(CH_2)_7CH_3$, 14H), 1.539 (m, $-CH_2(CH_2)_7CH_3$, 2H), 3.290 (m, –CONH*CH₂*–, 2H), 3.884 (s, –CO*CH₂*Br, 2H), 6.463 (br. s, amide –*NH*CO, 1H); ^{13}C NMR (100 MHz, $CDCl_3$): δ 14.247, 22.815, 26.953, 29.368, 29.405, 29.425, 29.559, 29.639, 29.652, 32.021, 40.443, 165.316.

2.3. General Synthesis of Cationic Small Molecules. *N,N,N′,N′*-Tetramethyl-α,ω-diaminoalkanes (5 mmol) was reacted with *N*-alkyl-1-bromoethanamide (15 mmol) in dry $CHCl_3$ (40 mL) in a screw-top pressure tube at 85 °C for about 24 h. After the reaction, the solvent was evaporated and the product was precipitated using excess diethylether. Finally the product was either filtered or washed or excess solvent was decanted and washed multiple times with diethylether. The precipitate was then dried overnight in vacuum oven at 55 °C to give **1a-1f**, **2a-2f** and **3a-3f** quantitatively.

1a: FT-IR: 3258 cm^{-1} (NH str.), 2920 cm^{-1} (CH_2 assym. str.), 2848 cm^{-1} (CH_2 sym. str.), 1685 cm^{-1} (amide I, C=O str.), 1550 cm^{-1} (amide II, NH ben.), 1472 cm^{-1} (CH_2 scissor); ^1H NMR (400 MHz, $CDCl_3$): δ 0.84 (t, terminal $-CH_3$, 6H), 1.26 (m, $-CH_2(CH_2)_7CH_3$, 28H), 1.52 (m, $-CH_2(CH_2)_7CH_3$, 4H), 3.21 (m, $-CONHCH_2-$, 4H), 3.61 (s, $-(CH_3)_2N^+-$, 12H), 4.68 (br. m, $-CH_2N^+Me_2-$, 4H), 4.81 (s, $-NHCOCH_2-$, 4H), 8.34 (br. s, amide –*NH*, 2H); ^{13}C NMR (100 MHz, $CDCl_3$): δ 14.1, 22.7, 27.1, 29.1, 29.3, 29.4, 29.6, 31.9, 40.1, 57.9, 63.0, 162.1; HRMS: calculated m/z 591.4207, 593.4188 $[M-Br^-]^+$, 256.2509 $[M-2Br^-]^{2+}$; observed m/z 591.4212, 593.4198 $[M-Br^-]^+$, 256.2529 $[M-2Br^-]^{2+}$.

1b: FT-IR: 3261 cm^{-1} (NH str.), 2928 cm^{-1} (CH_2 assym. str.), 2851 cm^{-1} (CH_2 sym. str.), 1682 cm^{-1} (amide I, C=O str.), 1554 cm^{-1} (amide II, NH ben.), 1476 cm^{-1} (CH_2 scissor); ^1H NMR (400 MHz, $CDCl_3$): δ 0.87 (t, terminal $-CH_3$, 6H), 1.29 (br. m, $-CH_2(CH_2)_7CH_3$, 28H), 1.55 (m, $-CH_2(CH_2)_7CH_3$, 4H), 2.21 (br. m, $-CH_2CH_2N^+Me_2-$, 4H), 3.27 (m, $-CONHCH_2-$, 4H), 3.45 (s, $-(CH_3)_2N^+-$, 12H), 3.89 (br. m, $-CH_2CH_2N^+Me_2-$, 4H), 4.44 (s, $-NHCOCH_2-$, 4H), 8.56 (br. s, amide –*NH*, 2H); ^{13}C NMR (100 MHz, $CDCl_3$): δ 14.2, 20.4, 22.7, 27.2, 29.2, 29.4, 29.4, 29.7, 31.9, 40.1, 63.1, 65.5, 162.6; HRMS: calculated m/z 619.4520, 621.4520 $[M-Br^-]^+$, 270.2665 $[M-2Br^-]^{2+}$; observed m/z 619.4525, 621.4521 $[M-Br^-]^+$, 270.2683 $[M-2Br^-]^{2+}$.

1c: FT-IR: 3255 cm^{-1} (NH str.), 2925 cm^{-1} (CH_2 assym. str.), 2852 cm^{-1} (CH_2 sym. str.), 1680 cm^{-1} (amide I, C=O str.), 1555 cm^{-1} (amide II, NH ben.), 1470 cm^{-1} (CH_2 scissor); ^1H NMR (400 MHz, $CDCl_3$): δ 0.87 (t, terminal $-CH_3$, 6H), 1.24-1.29 (m, $-CH_2(CH_2)_7CH_3$, 28H), 1.53-1.58 (m, $-CH_2(CH_2)_7CH_3$ and $-(CH_2)_2CH_2CH_2N^+Me_2$, 8H), 1.94 (br. m, $-CH_2CH_2N^+Me_2$, 4H), 3.25 (m, $-CONHCH_2-$, 4H), 3.44 (s, $-(CH_3)_2N^+-$, 12H), 3.75 (br. m, $-CH_2N^+Me_2-$, 4H), 4.57 (s, $-NHCOCH_2-$, 4H), 8.61 (br. s, amide –*NH*, 2H); ^{13}C NMR (100 MHz, $CDCl_3$): δ 14.2, 21.7, 22.7, 24.4, 27.2, 29.1, 29.4, 29.4, 29.6, 32.1, 40.1, 52.4, 62.9,

66.9, 162.9; HRMS: calculated m/z 647.4833, 649.4815, $[M–Br^–]^+$, 284.2822 $[M–2Br^–]^{2+}$; observed m/z 647.4830, 649.4813, $[M–Br^–]^+$, 284.2827 $[M–2Br^–]^{2+}$.

1d: FT-IR: 3257 cm^{-1} (NH str.), 2925 cm^{-1} (CH_2 assym. str.), 2849 cm^{-1} (CH_2 sym. str.), 1682 cm^{-1} (amide I, C=O str.), 1555 cm^{-1} (amide II, NH ben.), 1482 cm^{-1} (CH_2 scissor); ^1H NMR (400 MHz, $CDCl_3$): δ 0.87 (t, terminal $–CH_3$, 6H), 1.25-1.48 (m, $–CH_2(CH_2)_7CH_3$, 28H), 1.53-1.61 (m, $–(CH_2)_4CH_2CH_2N^+Me_2$, 8H), 1.96 (br. m, $–CH_2CH_2N^+Me_2$, 4H) 3.23 (m, –CONHCH_2–, 4H), 3.42 (s, $–(CH_3)_2N^+–$, 12H), 3.72 (br. m, $–(Me)_2^+NCH_2–$, 4H), 4.55 (s, –NHCOCH_2–, 4H), 8.74 (br. s, amide $–NH$, 2H); ^{13}C NMR (100 MHz, $CDCl_3$): δ 14.1, 21.7, 22.8, 24.5, 27.2, 29.2, 29.4, 29.5, 29.6, 32.1, 40.2, 52.5, 62.9, 66.9, 162.7; HRMS: calculated m/z 675.5148, 677.5130 $[M–Br^–]^+$, 298.2978 $[M–2Br^–]^{2+}$; observed m/z 675.5146, 677.5133 $[M–Br^–]^+$, 298.3002 $[M–2Br^–]^{2+}$.

1e: FT-IR: 3260 cm^{-1} (NH str.), 2920 cm^{-1} (CH_2 assym. str.), 2849 cm^{-1} (CH_2 sym. str.), 1682 cm^{-1} (amide I, C=O str.), 1555 cm^{-1} (amide II, NH ben.), 1477 cm^{-1} (CH_2 scissor); ^1H NMR (400 MHz, $CDCl_3$): δ 0.88 (t, terminal $–CH_3$, 6H), 1.27-1.35 (m, $–CH_2(CH_2)_7CH_3$ and $–CH_2(CH_2)_4CH_2CH_2N^+Me_2$, 32H), 1.43 (m, $–CH_2(CH_2)_4CH_2CH_2N^+Me_2$, 8H), 1.58 (m, $–CH_2(CH_2)_7CH_3$, 4H), 1.87 (br. m, $–CH_2CH_2N^+Me_2$, 4H), 3.26 (m, –CONHCH_2–, 4H), 3.39 (s, $–(CH_3)_2N^+–$, 12H), 3.70 (br. m, $–CH_2N^+Me_2–$, 4H), 4.57 (s, –NHCOCH_2–, 4H), 8.84 (br. s, amide $–NH$, 2H); ^{13}C NMR (100 MHz, $CDCl_3$): δ 14.2, 22.5, 22.8, 25.7, 27.2, 28.1, 28.2, 29.1, 29.3, 29.7, 32.1, 40.1, 52.1, 63.4, 66.9, 162.8; HRMS: calculated m/z 703.5459, 705.5450 $[M–Br^–]^+$, 312.3135 $[M–2Br^–]^{2+}$; observed m/z 703.5467, 705.5454 $[M–Br^–]^+$, 312.3177 $[M–2Br^–]^{2+}$.

1f: FT-IR: 3267 cm^{-1} (NH str.), 2931 cm^{-1} (CH_2 assym. str.), 2854 cm^{-1} (CH_2 sym. str.), 1688 cm^{-1} (amide I, C=O str.), 1550 cm^{-1} (amide II, NH ben.), 1480 cm^{-1} (CH_2 scissor); ^1H NMR (400 MHz, $CDCl_3$): δ 0.87 (t, terminal $–CH_3$, 6H), 1.25-1.30 (m, $–CH_2(CH_2)_5CH_3$ and

–*(CH$_2$)$_4$*(CH$_2$)$_4$CH$_2$CH$_2$N$^+$Me$_2$, 36H), 1.39 (m, –(CH$_2$)$_4$*(CH$_2$)$_4$*CH$_2$CH$_2$N$^+$Me$_2$, 8H), 1.56-1.61 (m, –*CH$_2$*(CH$_2$)$_5$CH$_3$, 4H), 1.85 (br. m, –*CH$_2$*CH$_2$N$^+$Me$_2$, 4H), 3.25 (m, –CONH*CH$_2$*–, 4H), 3.37 (s, –*(CH$_3$)$_2$*N$^+$–, 12H), 3.64 (br. m, –(Me)$_2^+$N*CH$_2$*–, 4H), 4.58 (s, –NHCO*CH$_2$*–, 4H), 8.88 (br. s, amide –*NH*, 2H); ^{13}C NMR (100 MHz, CDCl$_3$): δ 14.2, 22.4, 22.8, 25.7, 27.2, 28.1, 28.3, 29.2, 29.4, 29.7, 32.2, 41.1, 52.6, 63.5, 66.9, 162.7; HRMS: calculated m/z 731.5772, 733.5759 [M–Br$^-$]$^+$, 326.3291 [M–2Br$^-$]$^{2+}$; observed m/z 731.5776, 733.5761 [M–Br$^-$]$^+$, 326.3290 [M–2Br$^-$]$^{2+}$.

2a: FT-IR: 3260 cm^{-1} (NH str.), 2922 cm^{-1} (CH$_2$ assym. str.), 2850 cm^{-1} (CH$_2$ sym. str.), 1680 cm^{-1} (amide I, C=O str.), 1554 cm^{-1} (amide II, NH ben.), 1480 cm^{-1} (CH$_2$ scissor); ^{1}H NMR (400 MHz, CDCl$_3$): δ 0.87 (t, terminal –*CH$_3$*, 6H), 1.26-1.29 (m, –CH$_2$*(CH$_2$)$_5$*CH$_3$, 20H), 1.56-1.62 (m, –*CH$_2$*(CH$_2$)$_5$CH$_3$ and –*(CH$_2$)$_2$*CH$_2$CH$_2$N$^+$Me$_2$, 8H), 2.12 (br. m, –*CH$_2$*CH$_2$N$^+$Me$_2$, 4H) 3.21 (m, –CONH*CH$_2$*–, 4H), 3.61 (s, –*(CH$_3$)$_2$*N$^+$–, 12H), 4.68 (br. m, –(Me)$_2^+$N*CH$_2$*–, 4H), 4.81 (s, –NHCO*CH$_2$*–, 4H), 8.69 (br. s, amide –*NH*, 2H); ^{13}C NMR (100 MHz, CDCl$_3$): δ 14.1, 21.9, 22.7, 24.7, 27.1, 29.1, 29.2, 29.3, 31.8, 39.9, 62.9, 66.2, 162.9; HRMS: calculated m/z 591.4207, 593.4188 [M–Br$^-$]$^+$, 256.2509 [M–2Br$^-$]$^{2+}$; observed m/z 591.4214, 593.4202 [M–Br$^-$]$^+$, 256.2522 [M–2Br$^-$]$^{2+}$.

2b: FT-IR: 3259 cm^{-1} (NH str.), 2927 cm^{-1} (CH$_2$ assym. str.), 2854 cm^{-1} (CH$_2$ sym. str.), 1685 cm^{-1} (amide I, C=O str.), 1555 cm^{-1} (amide II, NH ben.), 1479 cm^{-1} (CH$_2$ scissor); ^{1}H NMR (400 MHz, CDCl$_3$): δ 0.87 (t, terminal –*CH$_3$*, 6H), 1.25-1.28 (br. m, –CH$_2$*(CH$_2$)$_5$*CH$_3$, 20H), 1.44 (m, –*(CH$_2$)$_4$*CH$_2$CH$_2$N$^+$Me$_2$, 8H), 1.58 (m, –*CH$_2$*(CH$_2$)$_5$CH$_3$, 4H), 1.95 (br. m, –*CH$_2$*CH$_2$N$^+$Me$_2$, 4H) 3.24 (m, –CONH*CH$_2$*–, 4H), 3.40 (s, –*(CH$_3$)$_2$*N$^+$–, 12H), 3.71 (br. m, –(Me)$_2^+$N*CH$_2$*–, 4H), 4.55 (s, –NHCO*CH$_2$*–, 4H), 8.79 (br. s, amide –*NH*, 2H); ^{13}C NMR (100 MHz, CDCl$_3$): δ 14.1, 22.3, 22.6, 25.5, 27.1, 27.7, 29.1, 29.2, 29.2, 31.8, 39.8, 52.2,

63.1, 66.2, 162.9; HRMS: calculated m/z 619.4520, 621.4520 $[M–Br^-]^+$, 270.2665 $[M–2Br^-]^{2+}$; observed m/z 619.4522, 621.4511 $[M–Br^-]^+$, 270.2679 $[M–2Br^-]^{2+}$.

2c: FT-IR: 3265 cm^{-1} (NH str.), 2927 cm^{-1} (CH_2 assym. str.), 2860 cm^{-1} (CH_2 sym. str.), 1675 cm^{-1} (amide I, C=O str.), 1550 cm^{-1} (amide II, NH ben.), 1474 cm^{-1} (CH_2 scissor); ^{1}H NMR (400 MHz, $CDCl_3$): δ 0.88 (t, terminal $–CH_3$, 6H), 1.26-1.31 (br. m, $–CH_2(CH_2)_5CH_3$, 20H), 1.57 (m, $–CH_2(CH_2)_5CH_3$, 4H), 3.23 (m, –CONHCH_2–, 4H), 3.62 (s, $–(CH_3)_2N^+$–, 12H), 4.68 (br. m, $–(Me)_2{}^+NCH_2$–, 4H), 4.81 (s, –NHCOCH_2–, 4H), 8.37 (br. s, amide –*NH*, 2H); ^{13}C NMR (100 MHz, $CDCl_3$): δ 14.2, 22.7, 27.1, 29.1, 29.3, 29.4, 31.9, 40.2, 53.1, 58.1, 63.1, 162.2; HRMS: calculated m/z 535.3581, 537.3569 $[M–Br^-]^+$, 228.2196 $[M–2Br^-]^{2+}$; observed m/z 535.3592, 537.3578 $[M–Br^-]^+$, 228.2203 $[M–2Br^-]^{2+}$.

2d: FT-IR: 3269 cm^{-1} (NH str.), 2933 cm^{-1} (CH_2 assym. str.), 2855 cm^{-1} (CH_2 sym. str.), 1685 cm^{-1} (amide I, C=O str.), 1555 cm^{-1} (amide II, NH ben.), 1480 cm^{-1} (CH_2 scissor); ^{1}H NMR (400 MHz, $CDCl_3$): δ 0.87 (t, terminal $–CH_3$, 6H), 1.26-1.34 (br. m, $–CH_2(CH_2)_5CH_3$, 20H), 1.44 (m, $–(CH_2)_4CH_2CH_2N^+Me_2$, 8H), 1.58 (m, $–CH_2(CH_2)_5CH_3$, 4H), 2.15 (br. m, $–CH_2CH_2N^+Me_2$, 4H) 3.23 (m, –CONHCH_2–, 4H), 3.46 (s, $–(CH_3)_2N^+$–, 12H), 3.92 (br. m, $–(Me)_2{}^+NCH_2$–, 4H), 4.47 (s, –NHCOCH_2–, 4H), 8.52 (br. s, amide –*NH*, 2H); ^{13}C NMR (100 MHz, $CDCl_3$): δ 14.2, 20.4, 22.7, 27.2, 29.1, 29.3, 29.3, 31.9, 40.1, 52.3, 63.1, 65.7, 162.6; HRMS: calculated m/z 563.3894, 565.3878 $[M–Br^-]^+$, 242.2352 $[M–2Br^-]^{2+}$; observed m/z 563.3895, 565.3881 $[M–Br^-]^+$, 242.2356 $[M–2Br^-]^{2+}$.

2e: FT-IR: 3260 cm^{-1} (NH str.), 2935 cm^{-1} (CH_2 assym. str.), 2855 cm^{-1} (CH_2 sym. str.), 1685 cm^{-1} (amide I, C=O str.), 1555 cm^{-1} (amide II, NH ben.), 1480 cm^{-1} (CH_2 scissor); ^{1}H NMR (400 MHz, $CDCl_3$): δ 0.87 (t, terminal $–CH_3$, 6H), 1.26-1.35 (br. m, $–CH_2(CH_2)_5CH_3$ and $–(CH_2)_4CH_2$CH2CH2N$^+$Me$_2$, 24H), 1.43 (m, $–(CH_2)_4$CH$_2$CH2CH2N$^+$Me$_2$, 8H), 1.54 (m, $–CH_2(CH_2)_5CH_3$, 4H), 1.87 (br. m, $–CH_2CH_2N^+Me_2$, 4H) 3.25 (m, –CONHCH_2–, 4H), 3.39

(s, $-(CH_3)_2N^+-$, 12H), 3.70 (br. m, $-(Me)_2{}^+NCH_2-$, 4H), 4.57 (s, –NHCOCH_2–, 4H), 8.84 (br. s, amide –*NH*, 2H); ^{13}C NMR (100 MHz, $CDCl_3$): δ 14.1, 22.7, 25.7, 27.1, 28.1, 28.2, 29.1, 29.3, 31.9, 40.1, 52.1, 63.4, 66.9, 162.8; HRMS: calculated m/z 647.4833, 649.4815, $[M–Br^-]^+$, 284.2822 $[M–2Br^-]^{2+}$; observed m/z 647.4835, 649.4819, $[M–Br^-]^+$, 284.2877 $[M–2Br^-]^{2+}$.

2f: FT-IR: 3263 cm^{-1} (NH str.), 2935 cm^{-1} (CH_2 assym. str.), 2860 cm^{-1} (CH_2 sym. str.), 1682 cm^{-1} (amide I, C=O str.), 1555 cm^{-1} (amide II, NH ben.), 1480 cm^{-1} (CH_2 scissor); ^{1}H NMR (400 MHz, $CDCl_3$): δ 0.86 (t, terminal –CH_3, 6H), 1.25-1.29 (br. m, $-CH_2(CH_2)_5CH_3$ and $-(CH_2)_8CH_2CH_2N^+Me_2$, 36H), 1.57 (m, $-CH_2(CH_2)_3CH_3$, 4H), 1.82 (br. m, $-CH_2CH_2N^+Me_2$, 4H) 3.26 (m, –CONHCH_2–, 4H), 3.38 (s, $-(CH_3)_2N^+-$, 12H), 3.66 (br. m, $-(Me)_2{}^+NCH_2-$, 4H), 4.57 (s, –NHCOCH_2–, 4H), 8.81 (br. s, amide –*NH*, 2H); ^{13}C NMR (100 MHz, $CDCl_3$): δ 14.1, 22.7, 22.9, 26.1, 27.2, 28.7, 28.8, 29.1, 29.3, 29.5, 29.6, 31.9, 39.9, 52.1, 63.4, 66.3, 162.8; HRMS: calculated m/z 675.5148, 677.5130 $[M–Br^-]^+$, 298.2978 $[M–2Br^-]^{2+}$; observed m/z 675.5148, 677.5133 $[M–Br^-]^+$, 298.3002 $[M–2Br^-]^{2+}$.

3a: FT-IR: 3257 cm^{-1} (NH str.), 2925 cm^{-1} (CH_2 assym. str.), 2850 cm^{-1} (CH_2 sym. str.), 1679 cm^{-1} (amide I, C=O str.), 1555 cm^{-1} (amide II, NH ben.), 1480 cm^{-1} (CH_2 scissor); ^{1}H NMR (400 MHz, $CDCl_3$): δ 0.87 (t, terminal –CH_3, 6H), 1.28-1.43 (m, $-CH_2(CH_2)_3CH_3$, and $-(CH_2)_6CH_2CH_2N^+Me_2$, 24H), 1.59 (m, $-CH_2(CH_2)_3CH_3$ 4H), 1.87 (br. m, $-CH_2CH_2N^+Me_2$, 4H) 3.25 (m, –CONHCH_2–, 4H), 3.39 (s, $-(CH_3)_2N^+-$, 12H), 3.68 (br. m, $-(Me)_2{}^+NCH_2-$, 4H), 4.56 (s, –NHCOCH_2–, 4H), 8.82 (br. s, amide –*NH*, 2H); ^{13}C NMR (100 MHz, $CDCl_3$): δ 14.1, 22.6, 22.6, 25.8, 26.7, 28.2, 28.4, 29.1, 31.4, 39.942, 52.1, 63.323, 66.4, 162.8; HRMS: calculated m/z 591.4207, 593.4188 $[M–Br^-]^+$, 256.2509 $[M–2Br^-]^{2+}$; observed m/z 591.4206, 593.4192 $[M–Br^-]^+$, 256.2524 $[M–2Br^-]^{2+}$.

3b: FT-IR: 3260 cm^{-1} (NH str.), 2928 cm^{-1} (CH_2 assym. str.), 2855 cm^{-1} (CH_2 sym. str.), 1680 cm^{-1} (amide I, C=O str.), 1555 cm^{-1} (amide II, NH ben.), 1480 cm^{-1} (CH_2 scissor); ^1H NMR (400 MHz, $CDCl_3$): δ 0.87 (t, terminal $–CH_3$, 6H), 1.28-1.39 (br. m, $–CH_2(CH_2)_3CH_3$ and $–(CH_2)_8CH_2CH_2N^+Me_2$, 28H), 1.56 (m, $–CH_2(CH_2)_3CH_3$, 4H), 1.83 (br. m, $–CH_2CH_2N^+Me_2$, 4H) 3.27 (m, –CONHCH_2–, 4H), 3.37 (s, $–(CH_3)_2N^+–$, 12H), 3.65 (br. m, $–(Me)_2^+NCH_2–$, 4H), 4.58 (s, –NHCOCH_2–, 4H), 8.89 (br. s, amide –*NH*, 2H); ^{13}C NMR (100 MHz, $CDCl_3$): δ 14.1, 22.6, 22.6, 22.9, 26.1, 26.5, 26.8, 28.6, 28.7, 28.7, 29.1, 29.3, 31.5, 40.1, 49.8, 52.1, 63.4, 162.8; HRMS: calculated m/z 619.4520, 621.4520 $[M–Br^–]^+$, 270.2665 $[M–2Br^–]^{2+}$; observed m/z 619.4527, 621.4516 $[M–Br^–]^+$, 270.2687 $[M–2Br^–]^{2+}$.

3c: FT-IR: 3263 cm^{-1} (NH str.), 2925 cm^{-1} (CH_2 assym. str.), 2852 cm^{-1} (CH_2 sym. str.), 1688 cm^{-1} (amide I, C=O str.), 1562 cm^{-1} (amide II, NH ben.), 1481 cm^{-1} (CH_2 scissor); ^1H NMR (400 MHz, $CDCl_3$): δ 0.88 (t, terminal $–CH_3$, 6H), 1.26-1.35 (m, $–CH_2(CH_2)_3CH_3$, 12H), 1.57 (m, $–CH_2(CH_2)_3CH_3$ 4H), 3.24 (m, –CONHCH_2–, 4H), 3.62 (s, $–(CH_3)_2N^+–$, 12H), 4.67 (br. m, $–(Me)_2^+NCH_2–$, 4H), 4.79 (s, –NHCOCH_2–, 4H), 8.81 (br. s, amide –*NH*, 2H); ^{13}C NMR (100 MHz, $CDCl_3$): δ 14.3, 22.6, 26.8, 29.1, 31.5, 40.2, 53.1, 63.2, 162.2; HRMS: calculated m/z 479.2955, 481.2940 $[M–Br^–]^+$, 200.1883 $[M–2Br^–]^{2+}$; observed m/z 479.2954, 481.2938 $[M–Br^–]^+$, 200.1886 $[M–2Br^–]^{2+}$.

3d: FT-IR: 3260 cm^{-1} (NH str.), 2928 cm^{-1} (CH_2 assym. str.), 2860 cm^{-1} (CH_2 sym. str.), 1681 cm^{-1} (amide I, C=O str.), 1556 cm^{-1} (amide II, NH ben.), 1484 cm^{-1} (CH_2 scissor); ^1H NMR (400 MHz, $CDCl_3$): δ 0.89 (t, terminal $–CH_3$, 6H), 1.26-1.29 (br. m, $–CH_2(CH_2)_3CH_3$ 12H), 1.54 (m, $–CH_2(CH_2)_3CH_3$, 4H), 2.14 (br. m, $–CH_2CH_2N^+Me_2$, 4H) 3.25 (m, –CONHCH_2–, 4H), 3.47 (s, $–(CH_3)_2N^+–$, 12H), 3.91 (br. m, $–(Me)_2^+NCH_2–$, 4H), 4.46 (s, –NHCOCH_2–, 4H), 8.51 (br. s, amide –*NH*, 2H); ^{13}C NMR (100 MHz, $CDCl_3$): δ 14.1, 20.4, 22.6, 26.7, 29.1, 31.4, 40.1, 52.2, 63.1, 65.5, 162.6; HRMS: calculated m/z 507.3268,

509.3291 $[M–Br^–]^+$, 214.2039 $[M–2Br^–]^{2+}$; observed m/z 507.3250, 509.3285 $[M–Br^–]^+$, 214.2063 $[M–2Br^–]^{2+}$.

3e: FT-IR: 3261 cm^{-1} (NH str.), 2925 cm^{-1} (CH_2 assym. str.), 2850 cm^{-1} (CH_2 sym. str.), 1680 cm^{-1} (amide I, C=O str.), 1560 cm^{-1} (amide II, NH ben.), 1482 cm^{-1} (CH_2 scissor); ^{1}H NMR (400 MHz, $CDCl_3$): δ 0.87 (t, terminal $–CH_3$, 6H), 1.26-1.37 (m, $–CH_2(CH_2)_3CH_3$, 12H), 1.55 (m, $–CH_2(CH_2)_3CH_3$ and $–(CH_2)_2CH_2CH_2N^+Me_2$, 8H), 2.1 (br. m, $–CH_2CH_2N^+Me_2$, 4H) 3.25 (m, –CONHCH_2–, 4H), 3.44 (s, $–(CH_3)_2N^+$–, 12H), 3.74 (br. m, $–(Me)_2^+NCH_2$–, 4H), 4.58 (s, –NHCOCH_2–, 4H), 8.61 (br. s, amide –*NH*, 2H); ^{13}C NMR (100 MHz, $CDCl_3$): δ 14.1, 21.8, 22.6, 24.5, 26.7, 29.1, 31.4, 39.9, 52.3, 62.8, 66.8, 162.8; HRMS: calculated m/z 535.3581, 537.3569 $[M–Br^–]^+$, 228.2196 $[M–2Br^–]^{2+}$; observed m/z 535.3593, 537.3576 $[M–Br^–]^+$, 228.2207 $[M–2Br^–]^{2+}$.

3f: FT-IR: 3260 cm^{-1} (NH str.), 2930 cm^{-1} (CH_2 assym. str.), 2860 cm^{-1} (CH_2 sym. str.), 1685 cm^{-1} (amide I, C=O str.), 1552 cm^{-1} (amide II, NH ben.), 1480 cm^{-1} (CH_2 scissor); ^{1}H NMR (400 MHz, $CDCl_3$): δ 0.87 (t, terminal $–CH_3$, 6H), 1.28-1.35 (br. m, $–CH_2(CH_2)_3CH_3$ 12H), 1.48 (m, $–CH_2(CH_2)_4CH_2$–, 8H), 1.59 (m, $–CH_2(CH_2)_3CH_3$, 4H), 1.95 (br. m, $–CH_2CH_2N^+Me_2$, 4H) 3.26 (m, –CONHCH_2–, 4H), 3.41 (s, $–(CH_3)_2N^+$–, 12H), 3.70 (br. m, $–(Me)_2^+NCH_2$–, 4H), 4.55 (s, –NHCOCH_2–, 4H), 8.76 (br. s, amide –*NH*, 2H); ^{13}C NMR (100 MHz, $CDCl_3$): δ 15.9, 24.5, 24.6, 27.8, 28.3, 30.4, 30.5, 33.2, 42.1, 54.9, 65.3, 67.8, 162.8; HRMS: calculated m/z 563.3894, 565.3878 $[M–Br^–]^+$, 242.2352 $[M–2Br^–]^{2+}$; observed m/z 563.3900, 565.3885 $[M–Br^–]^+$, 242.2359 $[M–2Br^–]^{2+}$.

3. *In-vitro* Antibacterial Assay

3.1. Minimum Inhibitory Concentration. The 6 h grown culture (~10^9 CFU/mL of bacteria) were diluted to give ~10^5 CFU/mL in respective media. Solutions of the small molecules were prepared in water and serial dilution was performed for all the compounds (2-fold serial

dilution). These dilutions (50 μL) were then added to the wells of 96-well plate followed by addition of 150 μL of previously made bacterial suspension (~10^5 CFU/mL). Two controls, one with only water and bacterial suspension and the other with compound solution with only media, were made. The plates were then incubated for 24 h at 37 °C. After incubation, optical density (OD) of the bacterial suspension was recorded using Plate Reader at 600 nm (TECAN, Infinite series, M200 pro). Each concentration was added in triplicate and all the experiments were repeated at least twice. Finally, antibacterial efficacy, expressed as minimum inhibitory concentration (MIC), was determined by considering the concentration at which the OD values were found to be similar to that of only media.

3.2. Biofilm Disruption Assay. Glass cover slips were sterilised by dipping them in ethanol and then drying in flame. The sterilised cover slips were placed in the wells of a 6-well plate. Bacteria (6 h grown) were then diluted to ~10^5 CFU/mL in nutrient medium supplemented with 1% glucose and 1% NaCl for *S. aureus* and M9 medium supplemented with 0.5% glycerol and 0.02% casamino acid for *E. coli* respectively and were added to the wells containing cover slips (2 mL). The well plate was then incubated under stationary conditions at 37 ˚C for about 24 h for *S. aureus* and 72 h for *E. coli* respectively. After incubation, medium was removed and planktonic bacteria were carefully washed once with PBS (pH = 7.4). Cover slips containing biofilms were then placed into the wells of another 6-well plate and 2 mL of test compound **3b** dissolved in the above respective media (at 32 μg/mL) was added to the wells containing the cover slips with already established bacterial biofilm. The plate was then allowed to incubate under stationary conditions at 37 ˚C for 24 h. Only 2 mL of the respective media was used as negative control. After 24 h, medium was discarded and cover slips were washed with PBS. Then trypsin-EDTA solution (100 μL) was added to the wells containing treated and non-treated cover slips to dissolve the biofilm matrix. Bacterial count was performed by serially diluting the suspension (10-fold dilution) and then plating on

nutrient agar plates. Bacterial colonies grown on the plate after 24 h were counted and viability of the cell within the matrix was expressed as $\log_{10}$ (CFU/mL). For imaging via CLSM, cover slips were stained with green fluorescent dye SYTO 9 (5 μM, 10 μL) and imaged using a confocal laser-scanning microscopy (Zeiss 510 Meta Confocal Microscope).

3.3. Minimum Biofilm Eradication Concentration (MBEC) Assay. The minimum biofilm eradication concentration for the cationic small molecules was determined following an earlier report.[18]

3.4. Membrane Hydration Assay. Lipids (0.5 mM DPPG:DPPE (88:12) or 0.5 mM of DPPC) and Laurdan dye (5 μM) were taken in glass vials in chloroform. Thin films were made under constant flow of dry argon gas. Films were then dried under vacuum. Finally, lipid films were hydrated with PBS (pH = 7.4) overnight. Hydrated films of lipids were then processed for 10 freeze thaw cycles from 70 °C to 4 °C with alternate vortexing. The solutions were then sonicated at 70 °C for 15 min to get unilamellar vesicles from multilamellar vesicles that form during vortexing. Laurdan dye embedded liposome (2 mL) (lipid: dye = 100:1) was taken in a fluorescence cuvette along with the compound solutions in PBS (pH = 7.4) (lipid: compound = 7.4:1). Fluorescence emission was then measured at 440 nm and 490 nm for an excitation wavelength at 350 nm. The measurements were performed using Water Peltier system attached PerkinElmer LS-55 Luminescence Spectrometer at 37 °C. Membrane hydration and hence changes in polarity are studied by shifts in the emission spectrum of Laurdan dye and are quantified by calculating the generalized polarization (GP).

GP was calculated by using the following equation.

$GP = (I_{440} - I_{490})/(I_{440} + I_{490})$ where I_{440} and I_{490} represent fluorescent emission intensity of the dye at 440 nm and 490 nm respectively for the excitation at 350 nm.

4. *In-vitro* Toxicity Assay

4.1. Hemolytic Assay. Studies on human subjects were performed according to the guidelines approved by Institutional Bio-Safety Committee (IBSC) at Jawaharlal Nehru Centre for Advanced Scientific Research (JNCASR). Blood was donated by a healthy human donor and red blood cells (RBCs) were isolated from the heparinised blood. The cells were then washed twice and finally resuspended in PBS (5 vol%). Cell suspension (150 μL) was then added to solutions of serially diluted small molecules taken in wells of a 96-well plate (50 μL). Two controls were prepared, one without the compounds (only 50 μL water) and the other with 0.1 vol% solution of Triton X-100 (TX, 50 μL). The plate was then incubated at 37 °C for 1 h. Next, cells were centrifuged at 3500 rpm for 5 minutes. Supernatant from the wells (~100 μL) was then transferred to a new 96-well plate and absorbance of the supernatant was recorded at 540 nm. Percentage of hemolysis was calculated as $(A–A_o)/(A_{total}–A_o)\times100$, where A is the absorbance for the test samples, A_o is the absorbance for the wells contained only water and RBC suspension , and A_{total} the absorbance of fully lysed cells (wells with TX), all at 540 nm.

4.2. Cytotoxicity Assay (Fluorescence Microscopy). Human embryo kidney (HEK 293) cells were seeded onto the wells of a tissue culture treated 96-well plate (~10^4 cells/well). The seeded cellswere then treated with the small molecules at 32 μg/mL. 0.1% Triton-X was used as positive control whereas untreated cells were used as negative controls. Both the treated and untreated cells were then washed once with PBS and stained with calcein AM (2 μM, Fluka) and propidium iodide (PI, 4.5 μM) (Sigma-Aldrich) for 15 min at 37 °C under 5% CO_2-95% atmosphere (50 μL of 1:1 calcein AM:PI). Finally, the cells were washed with PBS to remove the excess dyes and images were captured with a 20X objective in Leica DM2500 fluorescence microscope using. A band-pass filter for calcein AM at 500-550 nm and a long-pass filter for PI at 590-800 nm were used while imaging.

5. *In-vivo* Ttoxicity. *In-vivo* toxicity was determined according to the OECD guidelines (OECD 425) and following an earlier report.[21]

***6. In-vivo* Activity.** BALB/c mice (female, 6 to 8 weeks old, 18-22g) were used for the experiments. First, the mice were rendered neutropenic (~100 neutrophils/mL) by injecting two doses of cyclophosphamide intraperitoneally (i.p.) (150 mg/kg first dose and 100 mg/kg after 3 days of the first dose). After 24 h of the second dose, mice were anesthetized by ketamine-xylazine (40 mg/kg ketamine and 2 mg/kg) mixture i.p.) The back of each mouse was clipped and then shaved using a razor. While shaving, a wound (reddening and glistening of the skin without bleeding) was introduced on the dorsal midline of each mouse. To the wound site, methicillin-resistant *S. aureus* (MRSA) was added drop wise (~10^9 cells/mL, 20 μL) and allowed to dry to ensure that the bacteria remained within the shaved area. Mice (n = 5 in each group) were left for 24 h of the infection to allow to form the biofilm. Next, mice were treated with **3b** (40 mg/kg), fusidic acid (40 mg/kg), and ReliHeal-Silver ointment (Carboxymethylcellulose IP 3.5% w/w, colloidal silver nanoparticle 50 ppm, Reliance Life Advances, India) (200 mg/kg) at the site of infection. The compound solution was carefully added and spread on the entire wound surface to avoid any loss of solution. The dosages were continued for four days (per day one dose). One group of mice (n = 5) were left untreated and used as a control. Mice were sacrificed 18 h after the last dose using isofluorane and the infected skin was collected, homogenized, diluted and plated for cell counting. The bacterial count was finally expressed as log CFU/g of the tissue collected and expressed as mean ± standard error of mean. For imaging the skin tissue by SEM, some portion of skin tissue samples were fixed in formalin for 24 h, dried subsequently using 30, 50, 70, 90 and 100% ethanol. The skin tissue samples were then adhered on silicon wafers; sputter coated with gold and imaged by Quanta 3D FEG, FEI field emission scanning electron microscope.

ANCILLARY INFORMATION

Supporting Information

^{1}H NMR and high resolution mass spectra, figures showing fluorescence microscopy of mammalian cells, table showing antibiofilm activity. The Supporting Information is available free of charge on the ACS Publications website.

Acknowledgements

We thank Prof. C. N. R. Rao, FRS for constant support and guidance. J. Hoque thanks JNCASR for senior research fellowship (SRF).

Abbreviation Used:

FT-IR = Fourier Transform Infrared Spectroscopy
NMR = Nuclear Magnetic Resonance
HRMS = High Resolution Mass Spectrometry
SEM = Scanning Electron Microscopy
HPLC = High Performance Liquid Chromatography
PBS = Phosphate-buffered Saline
MIC = Minimum Inhibitory Concentration
MBEC = Minimum Biofilm Eradication Concentration
MRSA = Methicillin-resistant *Staphylococcus aureus*
CFU = Colony Forming Unit
PI = Propidium Iodide
HEK = Human Embryonic Kidney
TX = Triton X
HC_{50} = 50% Hemolytic Concentration
LD_{50} = 50% Lethal Dose

Author Information

*Corresponding author: jayanta@jncasr.ac.in; Tel: +91-080-2208-2565

Notes

The authors declare no competing financial interests.

References

1. Hetrick, E. M.; Schoenfisch, M. H. Reducing Implant-related Infections: Active Release Strategies. *Chem. Soc. Rev.* **2006,** *35*, 780-789.

2. Hall-Stoodley, L.; Costerton, J. W.; Stoodley, P. Bacterial Biofilms: From the Natural Environment to Infectious Diseases. *Nat. Rev. Microbiol.* **2004,** *2*, 95-108.

3. Costerton, J. W.; Stewart, P. S.; Greenberg, E. P. Bacterial Biofilms: A Common Cause of Persistent Infections. *Science* **1999,** *284*, 1318-1322.

4. Arciola, C. R.; Campoccia, D.; Speziale, P.; Montanaro, L.; Costerton, J. W. Biofilm Formation in Staphylococcus Implant Infections. A Review of Molecular Mechanisms and Implications for Biofilm-resistant Materials. *Biomaterials* **2012,** *33*, 5967-5982.

5. Costerton, J. W.; Montanaro, L.; Arciola, C. R. Biofilm in Implant Infections: Its Production and Regulation. *Int. J. Artif. Organs* **2005,** *28*, 1062-1068.

6. Cho, H. S.; Lee, J.-H.; Ryu, S. Y.; Joo, S. W.; Cho, M. H.; Lee, J. Inhibition of *Pseudomonas aeruginosa* and *Escherichia coli* O157:H7 Biofilm Formation by Plant Metabolite ε-Viniferin. *J. Agric. Food Chem.* **2013**, *61*, 7120-7126.

7. Joseph, R.; Naugolny, A.; Feldman, M.; Herzog, I. M.; Fridman, M.; Cohen, Y. Cationic Pillararenes Potently Inhibit Biofilm Formation without Affecting Bacterial Growth and Viability. *J. Am. Chem. Soc.* **2016,** *138*, 754-757.

8. Reymond, J. L.; Bergmann, M.; Darbre, T. Glycopeptide Dendrimers as *Pseudomonas aeruginosa* Biofilm Inhibitors. *Chem. Soc. Rev.* **2013,** *42*, 4814-4822.

9. Geske, G. D.; Wezeman, R. J.; Siegel, A. P.; Blackwell, H. E. Small Molecule Inhibitors of Bacterial Quorum Sensing and Biofilm Formation. *J. Am. Chem. Soc.* **2005,** *127*, 12762-12763.

10. Huigens, R. W.; Richards, J. J.; Parise, G.; Ballard, T. E.; Zeng, W.; Deora, R.; Melander, C. Inhibition of *Pseudomonas aeruginosa* Biofilm Formation with Bromoageliferin Analogues. *J. Am. Chem. Soc.* **2007,** *129*, 6966-6967.

11. de la Fuente-Nunez, C.; Korolik, V.; Bains, M.; Nguyen, U.; Breidenstein, E. B. M.; Horsman, S.; Lewenza, S.; Burrows, L.; Hancock, R. E. W. Inhibition of Bacterial Biofilm Formation and Swarming Motility by a Small Synthetic Cationic Peptide. *Antimicrob. Agents Chemother.* **2012,** *56*, 2696-2704.

12. Shetye, G. S.; Singh, N.; Jia, C. Q.; Nguyen, C. D. K.; Wang, G. R.; Luk, Y. Y. Specific Maltose Derivatives Modulate the Swarming Motility of Nonswarming Mutant and Inhibit Bacterial Adhesion and Biofilm Formation by *Pseudomonas aeruginosa*. *ChemBioChem* **2014,** *15*, 1514-1523.

13. Peng, L. L.; DeSousa, J.; Su, Z. M.; Novak, B. M.; Nevzorov, A. A.; Garland, E. R.; Melander, C. Inhibition of *Acinetobacter baumannii* Biofilm Formation on a Methacrylate Polymer Containing a 2-Aminoimidazole Subunit. *Chem. Commun.* **2011,** *47*, 4896-4898.

14. Hoiby, N.; Bjarnsholt, T.; Givskov, M.; Molin, S.; Ciofu, O. Antibiotic Resistance of Bacterial Biofilms. *Int. J. Antimicrob. Agents* **2010,** *35*, 322-332.

15. Davies, D. Understanding Biofilm Resistance to Antibacterial Agents. *Nat. Rev. Drug Discov.* **2003,** *2*, 114-122.

16. Stewart, P. S.; Costerton, J. W. Antibiotic Resistance of Bacteria in Biofilms. *Lancet* **2001,** *358*, 135-138.

17. Bottcher, T.; Kolodkin-Gal, I.; Kolter, R.; Losick, R.; Clardy, J. Synthesis and Activity of Biomimetic Biofilm Disruptors. *J. Am. Chem. Soc.* **2013,** *135*, 2927-2930.

18. Konai, M. M.; Haldar, J. Lysine-Based Small Molecules That Disrupt Biofilms and Kill both Actively Growing Planktonic and Nondividing Stationary Phase Bacteria. *ACS Infect. Dis.* **2015,** *1*, 469-478.

19. Jennings, M. C.; Ator, L. E.; Paniak, T. J.; Minbiole, K. P. C.; Wuest, W. M. Biofilm-Eradicating Properties of Quaternary Ammonium Amphiphiles: Simple Mimics of Antimicrobial Peptides. *ChemBioChem* **2014,** *15*, 2211-2215.

20. Hoque, J.; Konai, M. M.; Samaddar, S.; Gonuguntala, S.; Manjunath, G. B.; Ghosh, C.; Haldar, J. Selective and Broad Spectrum Amphiphilic Small Molecules to Combat Bacterial Resistance and Eradicate Biofilms. *Chem. Commun.* **2015,** *51*, 13670-13673.

21. Ghosh, C.; Manjunath, G. B.; Konai, M. M.; Uppu, D. S.; Hoque, J.; Paramanandham, K.; Shome, B. R.; Haldar, J. Aryl-Alkyl-Lysines: Agents That Kill Planktonic Cells, Persister Cells, Biofilms of MRSA and Protect Mice from Skin-Infection. *Plos One* **2015,** *10*, e0144094.

22. Oppenheimer-Shaanan, Y.; Steinberg, N.; Kolodkin-Gal, I. Small Molecules are Natural Triggers for the Disassembly of Biofilms. *Trends Microbiol.* **2013,** *21*, 594-601.

23. Slomberg, D. L.; Lu, Y.; Broadnax, A. D.; Hunter, R. A.; Carpenter, A. W.; Schoenfisch, M. H. Role of Size and Shape on Biofilm Eradication for Nitric Oxide-Releasing Silica Nanoparticles. *ACS Appl. Mater. Interfaces* **2013**, *5*, 9322-9329.

24. Barraud, N.; Kardak, B. G.; Yepuri, N. R.; Howlin, R. P.; Webb, J. S.; Faust, S. N.; Kjelleberg, S.; Rice, S. A.; Kelso, M. J. Cephalosporin-3 '-diazeniumdiolates: Targeted NO-Donor Prodrugs for Dispersing Bacterial Biofilms. *Angew. Chem. Int. Ed.* **2012,** *51*, 9057-9060.

25. Goswami, S.; Thiyagarajan, D.; Das, G.; Ramesh, A. Biocompatible Nanocarrier Fortified with a Dipyridinium-Based Amphiphile for Eradication of Biofilm. *ACS Appl. Mater. Interfaces* **2014**, *6*, 16384-16394.

26. Duncan, B.; Li, X.; Landis, R. F.; Kim, S. T.; Gupta, A.; Wang, L.-S.; Ramanathan, R.; Tang, R.; Boerth, J. A.; Rotello. V. M. Nanoparticle-Stabilized Capsules for the Treatment of Bacterial Biofilms. *ACS Nano* **2015**, *9*, 7775-7782.

27. Konai, M. M.; Adhikary, U.; Samaddar, S.; Ghosh, C.; Haldar, J. Structure Activity Relationship of Amino Acid Tunable Lipidated Norspermidine Conjugates: Disrupting Biofilms with Potent Activity against Bacterial Persisters. *Bioconjugate Chem.* **2015**, *26*, 2442-2453.

28. Frei, R.; Breitbach, A. S.; Blackwell, H. E. 2-Aminobenzimidazole Derivatives Strongly Inhibit and Disperse *Pseudomonas aeruginosa* Biofilms. *Angew. Chem. Int. Ed.* **2012,** *51*, 5226-5229.

29. Hoque, J.; Konai, M. M.; Gonuguntla, S.; Manjunath, G. B.; Samaddar, S.; Yarlagadda, V.; Haldar, J. Membrane Active Small Molecules Show Selective Broad Spectrum Antibacterial Activity with No Detectable Resistance and Eradicate Biofilms. *J. Med. Chem.* **2015,** *58*, 5486-5500.

30. Rogers, S. A.; Huigens, R. W., Melander, C. A 2-Aminobenzimidazole that Inhibits and Disperses Gram-positive Biofilms through a Zinc-dependent Mechanism. *J. Am. Chem. Soc.* **2009,** *131*, 9868-9869.

31. Richards, J. J.; Huigens Iii, R. W.; Ballard, T. E.; Basso, A.; Cavanagh, J.; Melander, C. Inhibition and Dispersion of Proteobacterial Biofilms. *Chem. Commun.* **2008**, *44*, 1698-1700.

32. Hoque, J.; Akkapeddi, P.; Yarlagadda, V.; Uppu, D. S.; Kumar, P.; Haldar, J. Cleavable Cationic Antibacterial Amphiphiles: Synthesis, Mechanism of Action, and Cytotoxicities. *Langmuir* **2012,** *28*, 12225-12234.

33. Lee, M. R.; Raman, N.; Gellman, S. H.; Lynn, D. M.; Palecek, S. P. Hydrophobicity and Helicity Regulate the Antifungal Activity of 14-Helical beta-Peptides. *ACS Chem. Biol.* **2014,** *9*, 1613-1621.

34. Radzishevsky, I. S.; Rotem, S.; Bourdetsky, D.; Navon-Venezia, S.; Carmeli, Y.; Mor, A. Improved Antimicrobial Peptides based on Acyl-lysine Oligomers. *Nat. Biotechnol.* **2007,** *25*, 657-659.

35. Chongsiriwatana, N. P.; Patch, J. A.; Czyzewski, A. M.; Dohm, M. T.; Ivankin, A.; Gidalevitz, D.; Zuckermann, R. N.; Barron, A. E. Peptoids that Mimic the Structure, Function, and Mechanism of Helical Antimicrobial Peptides. *Proc. Natl. Acad. Sci. U. S. A.* **2008,** *105*, 2794-2799.

36. Jennings, M. C.; Minbiole, K. P. C.; Wuest, W. M. Quaternary Ammonium Compounds: An Antimicrobial Mainstay and Platform for Innovation to Address Bacterial Resistance. *ACS Infect. Dis.* **2015,** *1*, 288-303.

37. Thaker, H. D.; Som, A.; Ayaz, F.; Lui, D.; Pan, W.; Scott, R. W.; Anguita, J.; Tew, G. N. Synthetic Mimics of Antimicrobial Peptides with Immunomodulatory Responses. *J. Am. Chem. Soc.* **2012,** *134*, 11088-11091.

38. Albada, H. B.; Prochnow, P.; Bobersky, S.; Langklotz, S.; Schriek, P.; Bandow, J. E.; Metzler-Nolte, N. Tuning the Activity of a Short Arg-Trp Antimicrobial Peptide by Lipidation of a C- or N-Terminal Lysine Side-Chain. *ACS Med. Chem. Lett.* **2012**, *3*, 980-984.

39. Sambhy, V.; Peterson, B. R.; Sen, A. Antibacterial and Hemolytic Activities of Pyridinium Polymers as a Function of the Spatial Relationship between the Positive Charge and the Pendant Alkyl Tail. *Angew. Chem. Int. Ed.* **2008,** *47*, 1250-1254.

40. Berkov-Zrihen, Y.; Herzog, I. M.; Feldman, M.; Fridman, M. Site-selective Displacement of Tobramycin Hydroxyls for Preparation of Antimicrobial Cationic Amphiphiles. *Org. Lett.* **2013,** *15*, 6144-6147.

41. Wang, Y.; Chen, F.; Di, H.; Xu, Y.; Xiao, Q.; Wang, X.; Wei, H.; Lu, Y.; Zhang, L.; Zhu, J.; Sheng, C.; Lan, L.; Li, J. Discovery of Potent Benzofuran-Derived Diapophytoene

Desaturase (CrtN) Inhibitors with Enhanced Oral Bioavailability for the Treatment of Methicillin-Resistant *Staphylococcus aureus* (MRSA) Infections. *J. Med. Chem.* **2016**, *59*, 3215-3230.

42. Wang, B.; Pachaiyappan, B.; Gruber, J. D.; Schmidt, M. G.; Zhang, Y. M.; Woster, P. M. Antibacterial Diamines Targeting Bacterial Membranes. *J. Med. Chem.* **2016,** *59*, 3140-3151.

43. Teng, P.; Huo, D.; Nimmagadda, A.; Wu, J.; She, F.; Su, M.; Lin, X.; Yan, J.; Cao, A.; Xi, C.; Hu, Y.; Cai, J. Small Antimicrobial Agents Based on Acylated Reduced Amide Scaffold. *J. Med. Chem.* **2016,** *59*, 7877-7887.

44. Stec, J.; Onajole, O. K.; Lun, S. C.; Guo, H. D.; Merenbloom, B.; Vistoli, G.; Bishai, W. R.; Kozikowski, A. P. Indole-2-carboxamide-based MmpL3 Inhibitors Show Exceptional Antitubercular Activity in an Animal Model of Tuberculosis Infection. *J. Med. Chem.* **2016,** *59*, 6232-6247.

45. Makovitzki, A.; Avrahami, D.; Shai, Y. Ultrashort Antibacterial and Antifungal Lipopeptides. *Proc. Natl. Acad. Sci. U. S. A.* **2006,** *103*, 15997-16002.

46. Forman, M. E.; Jennings, M. C.; Wuest, W. M.; Minbiole, K. P. Building A Better Quaternary Ammonium Compound (QAC): Branched Tetracationic Antiseptic Amphiphiles. *ChemMedChem* **2016,** *11*, 1401-1405.

47. Uppu, D. S. S. M.; Konai, M. M.; Baul, U.; Singh, P.; Siersma, T. K.; Samaddar, S.; Vemparala, S.; Hamoen, L. W.; Narayana, C.; Haldar, J. Isosteric Substitution in Cationic-Amphiphilic Polymers Reveals an Important Role for Hydrogen Bonding in Bacterial Membrane Interactions. *Chem. Sci.* **2016,** *7*, 4613-4623.

48. Wiegand, I.; Hilpert, K.; Hancock, R. E. W. Agar and Broth Dilution Methods to Determine the Minimal Inhibitory Concentration (MIC) of Antimicrobial Substances. *Nat. Protoc.* **2008,** *3*, 163-175.

49. Ivankin, A.; Livne, L.; Mor, A.; Caputo, G. A.; Degrado, W. F.; Meron, M.; Lin, B.; Gidalevitz, D. Role of the Conformational Rigidity in the Design of Biomimetic Antimicrobial Compounds. *Angew. Chem. Int. Ed.* **2010,** *49*, 8462-8465.

50. Wieprecht, T.; Apostolov, O.; Beyermann, M.; Seelig, J. Membrane Binding and Pore Formation of the Antibacterial Peptide PGLa: Thermodynamic and Mechanistic Aspects. *Biochemistry* **2000,** *39*, 442-452.

51. Roversi, D.; Luca, V.; Aureli, S.; Park, Y.; Mangoni, M. L.; Stella, L. How Many AMP Molecules Kill a Bacterium? The Case of PMAP-23. *ACS Chem. Biol.* **2014**, *9*, 2003-2007.

52. Yarlagadda, V.; Samaddar, S.; Paramanandham, K.; Shome, B. R.; Haldar, J., Membrane Disruption and Enhanced Inhibition of Cell-Wall Biosynthesis: A Synergistic Approach to Tackle Vancomycin-Resistant Bacteria. *Angew. Chem. Int. Ed.* **2015,** *54*, 13644-13649.

53. Uppu, D. S. S. M.; Bhowmik, M.; Samaddar, S.; Haldar, J. Cyclization and Unsaturation Rather than Isomerisation of Side Chains Govern the Selective Antibacterial Activity of Cationic-Amphiphilic Polymers. *Chem. Commun.* **2016,** *52*, 4644-4647.

54. Uppu, D. S. S. M.; Samaddar, S.; Ghosh, C.; Paramanandham, K.; Shome, B. R.; Haldar, J. Amide Side Chain Amphiphilic Polymers Disrupt Surface Established Bacterial Biofilms and Protect Mice from Chronic *Acinetobacter baumannii* Infection. *Biomaterials* **2016,** *74*, 131-143.

55. Donlan, R. M.; Costerton, J. W. Biofilms: Survival Mechanisms of Clinically Relevant Microorganisms. *Clin. Microbiol. Rev.* **2002,** *15*, 167-193.

56. Ghosh, C.; Manjunath, G. B.; Konai, M. M.; Uppu, D. S. S. M.; Paramanandham, K.; Shome, B. R.; Ravikumar, R.; Haldar, J. Aryl-alkyl-lysines: Membrane-Active Small Molecules Active against Murine Model of Burn Infection. *ACS Infect. Dis.* **2016,** *2*, 111-122.

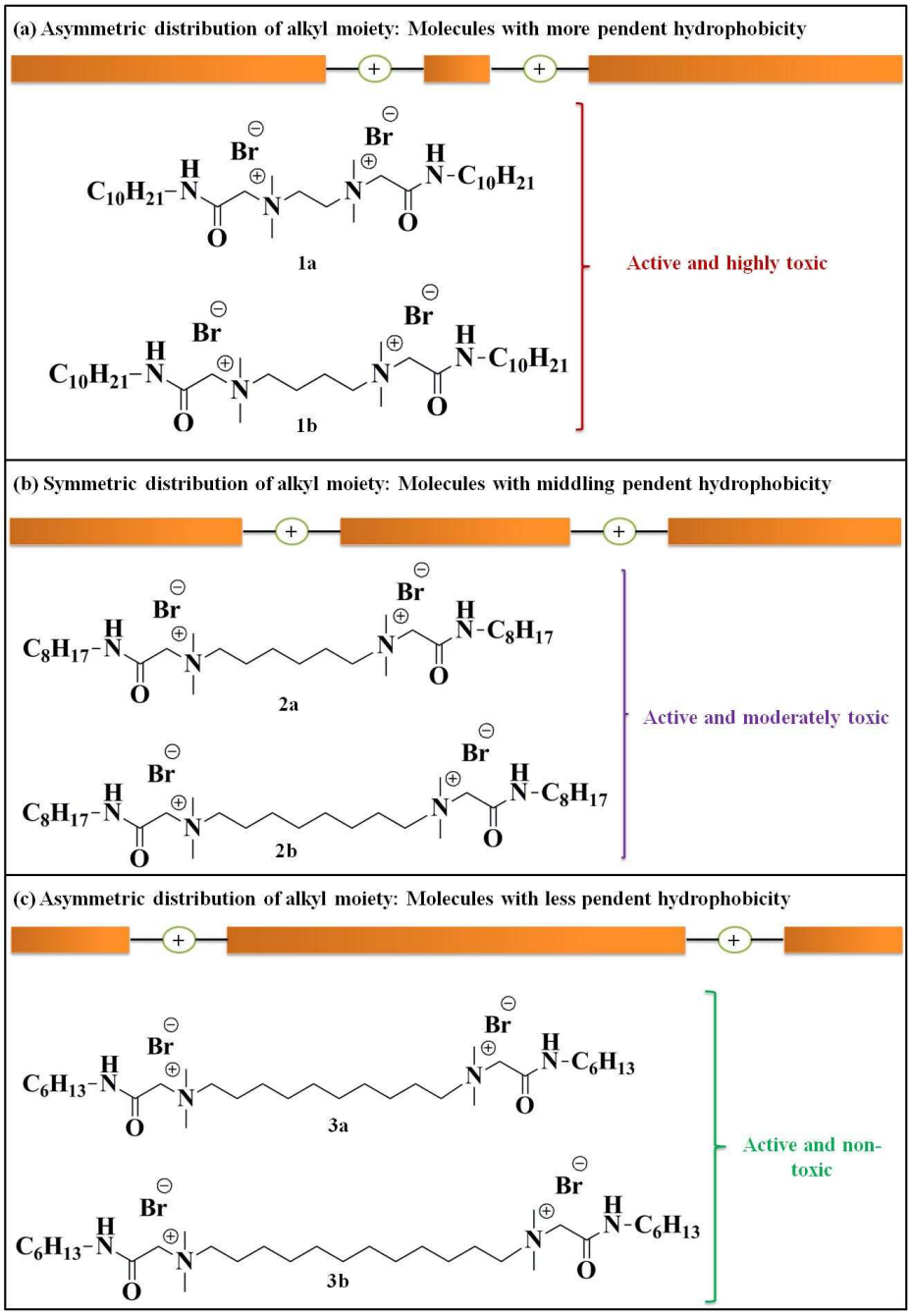

Figure 1. Structures of cationic small molecules with spatial control of hydrophobicity. Dark orange color represents length of the hydrophobic moiety.

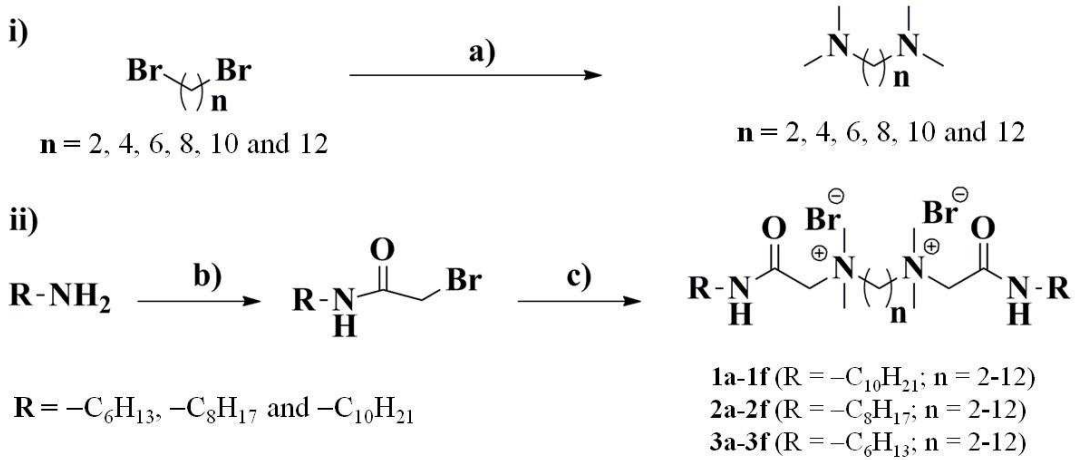

Scheme 1. Synthesis of cationic small molecules. (a) i) $NHMe_2$, $CHCl_3$, RT, 24 h; i) aq NaOH (2M); (b) $BrCH_2COBr$, K_2CO_3, DCM, H_2O; 5 ˚C (30 min), RT (4 h); (c) $Me_2N(CH_2)_nNMe_2$, $CHCl_3$, pressure tube, 85 ˚C, 24 h.

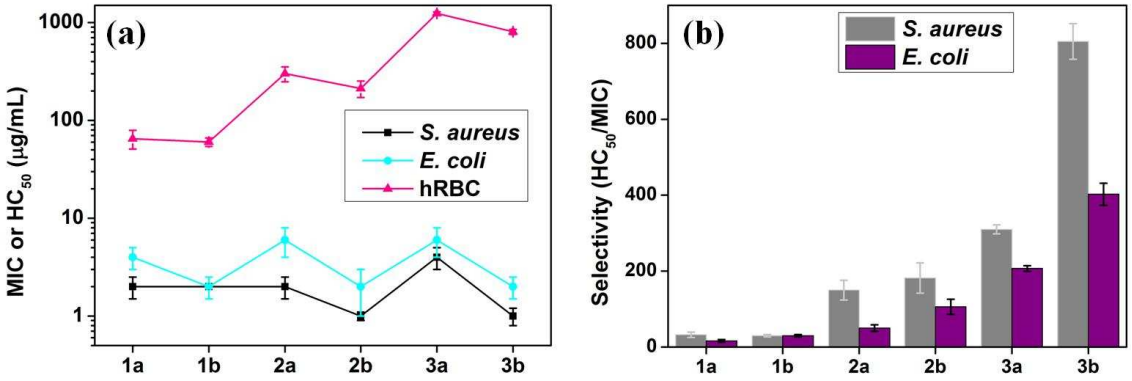

Figure 2. Biological activity of the small molecules that differ only in spatial positioning: (a) antibacterial and hemolytic activities of the molecules; (b) selectivity of the molecules.

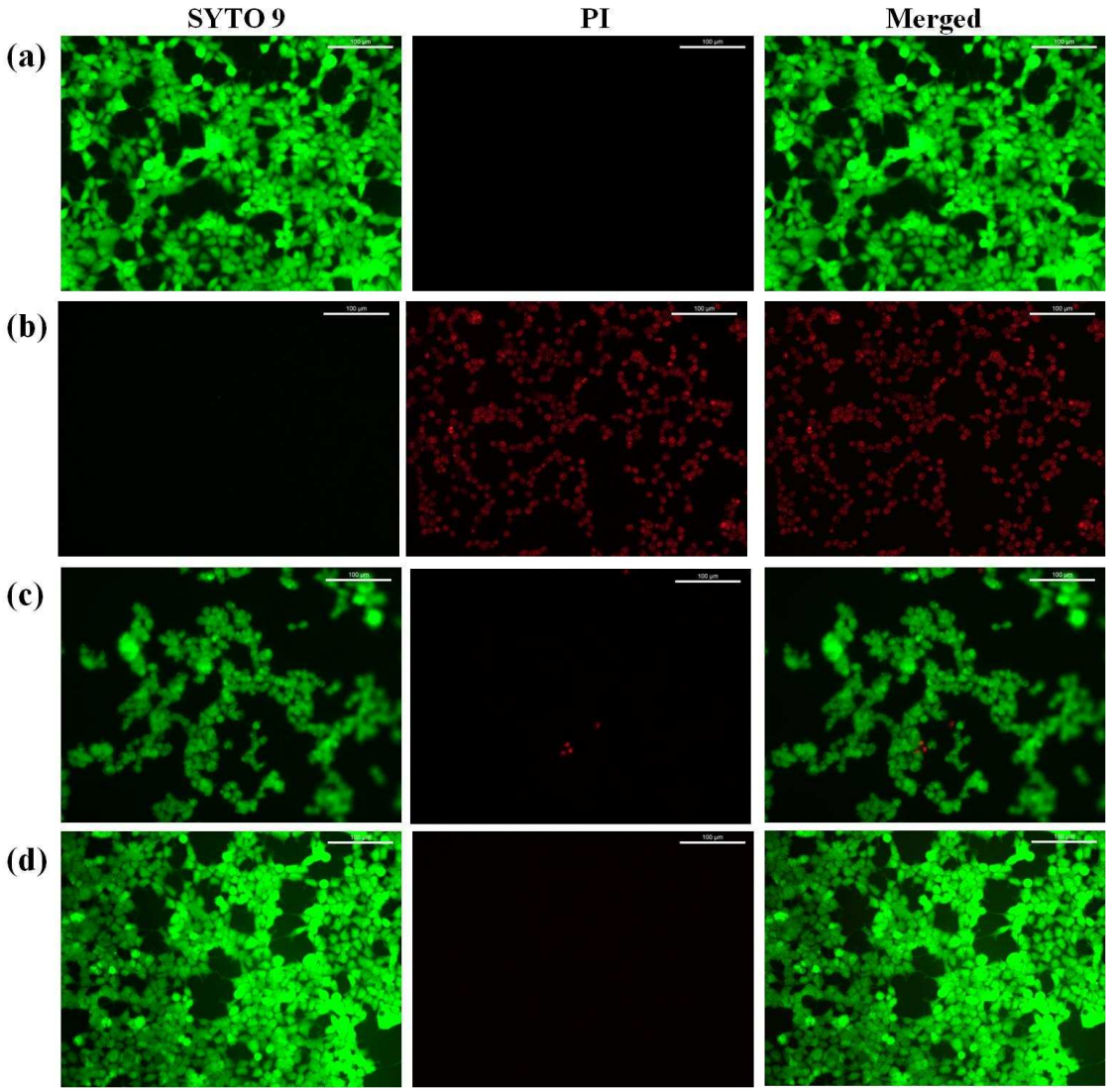

Figure 3. Cytotoxicity of the small molecules. Fluorescence microscopy images of HEK 293 cells after treatment with molecules for 24 h and staining with calcein AM and PI. Panel (a): non-treated cells (negative control); panel (b): cells treated with **1b**; panel (c): cells treated with **2b**; (d) cells treated with **3b**, all at 32 μg/mL respectively.

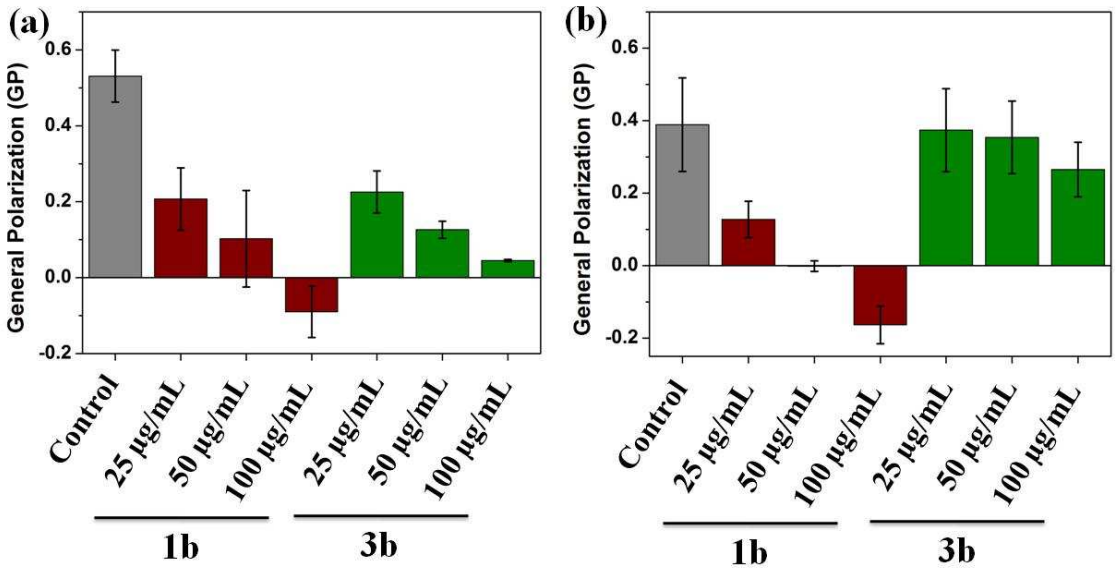

Figure 4. Membrane hydration of lipid bilayers consisting of (a) DPPG:DPPE (88:12) liposome and (b) DPPC liposome treated with small molecules **1b** and **3b**.

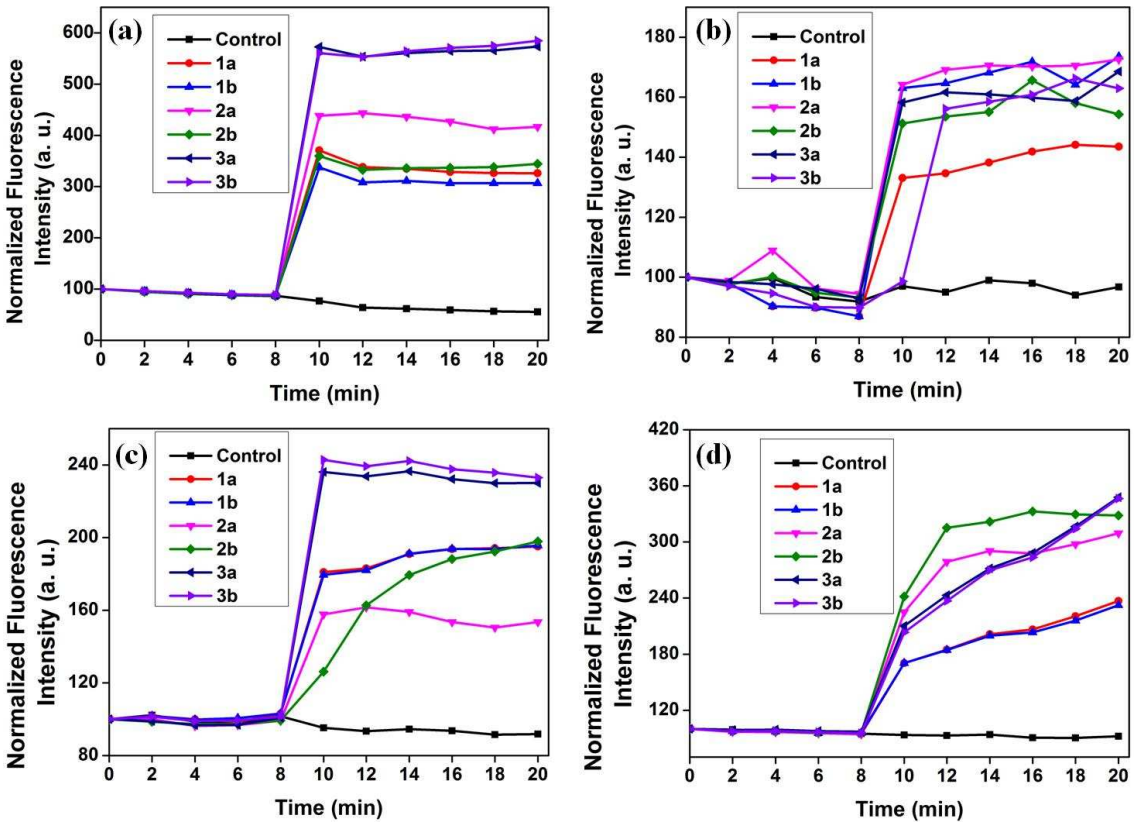

Figure 5. Membrane-active mode of action of cationic small molecules. Membrane depolarization of (a) *S. aureus* and (b) *E. coli* and membrane permeabilization of (c) *S. aureus* and (d) *E. coli* respectively in the presence of cationic molecules (all at 32 μg/mL).

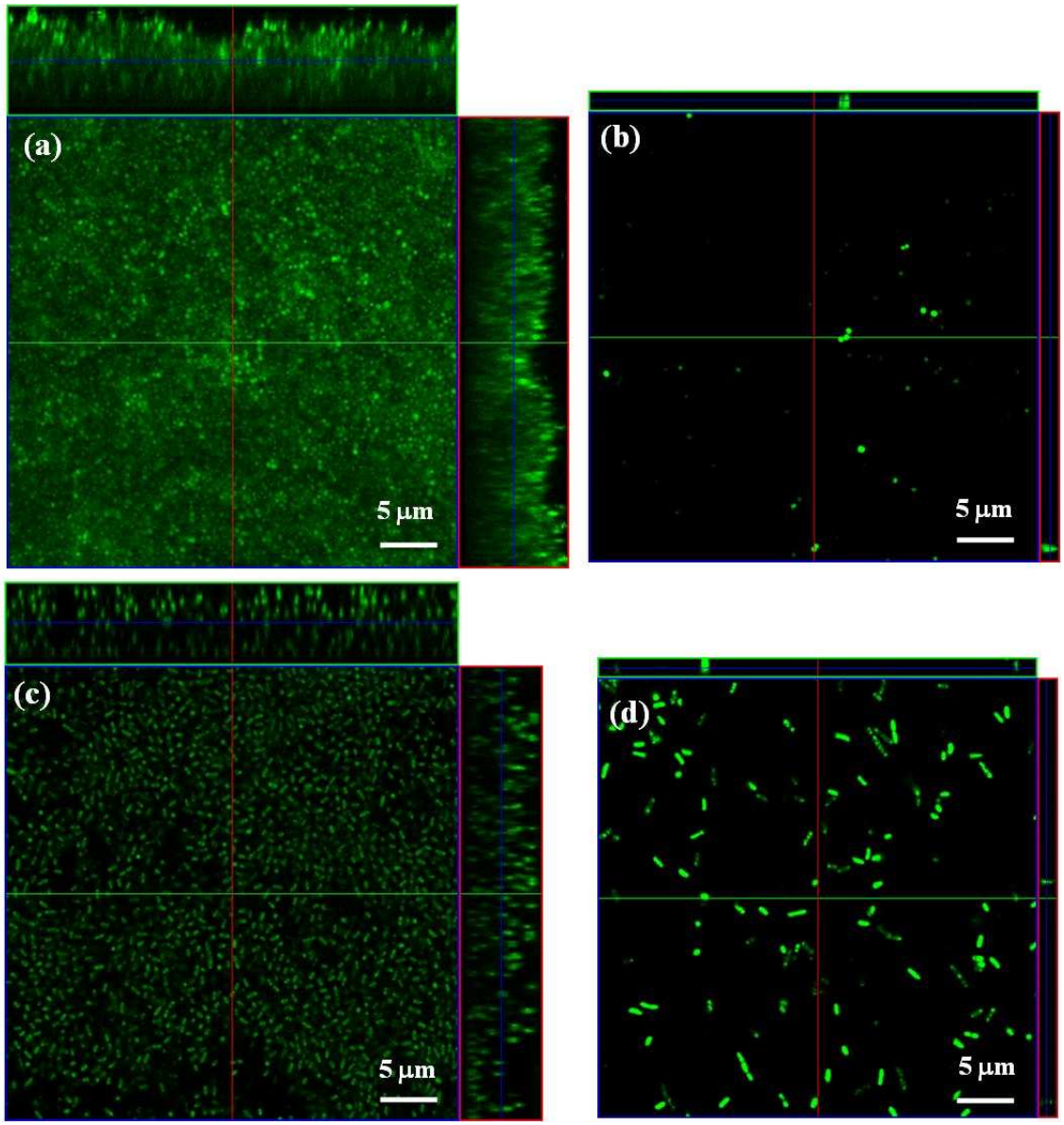

Figure 6. *In-vitro* antibiofilm efficacy of molecule **3b**. CLSM images of (a and c) non-treated *S. aureus* and *E. coli* biofilm; (b and d) **3b** treated *S. aureus* and *E. coli* biofilm (at 32 μg/mL) after staining with SYTO 9.

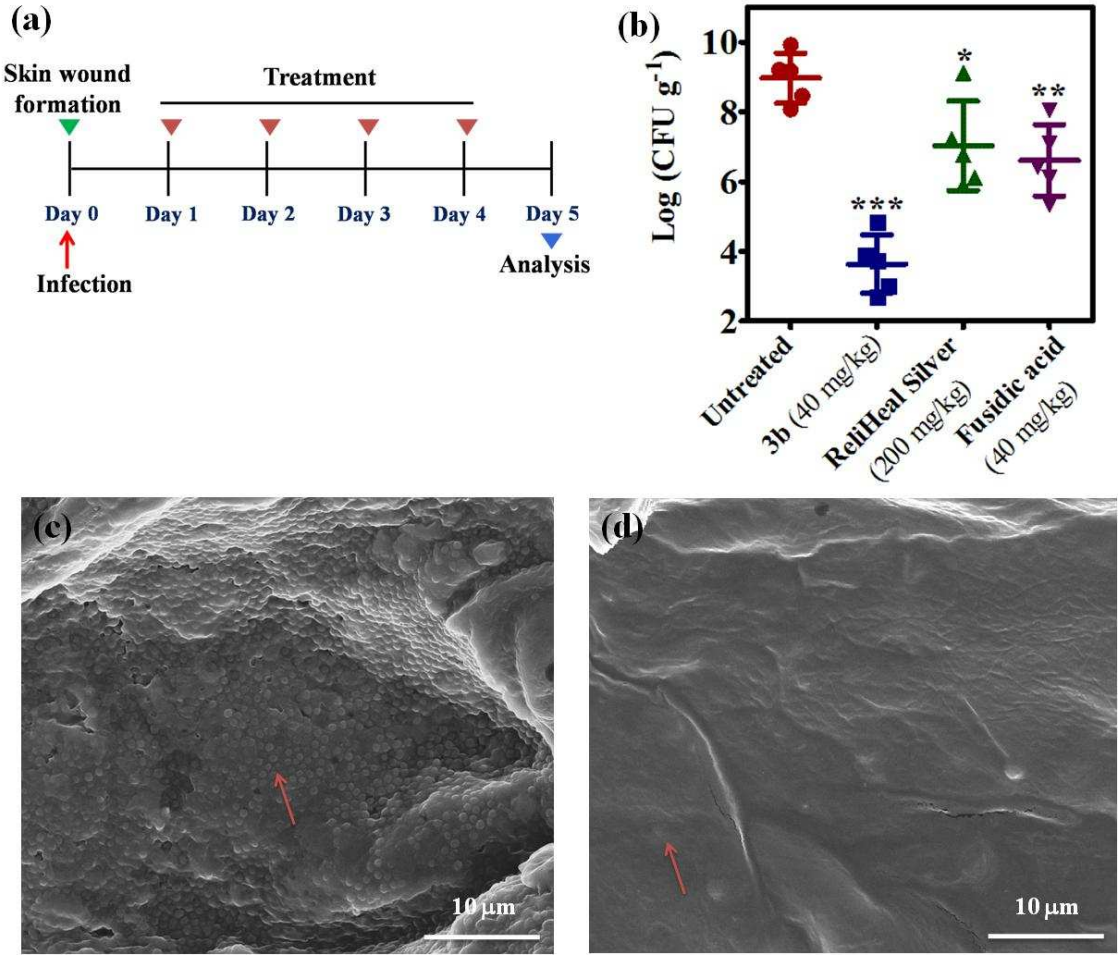

Figure 7. *In-vivo* activity and antibiofilm efficacy of **3b**. (a) Experimental plan of murine model of superficial MRSA biofilm formation and treatment after mice were rendered neutropenic; (b) bacterial count of the treated and un-treated skin tissue sample from mice. Scanning electron microscopy images of the skin tissue samples representing bacteria (c) after 24 h of infection and (d) after 4 days of treatment with **3b** (at 40 mg/kg). Arrow indicates the bacterial cells; p values (*) are <0.0001, 0.0183 and 0.0025 for **3b**-, Reliheal silver- and fusidic acid- treated samples.

Table 1. Antibacterial and hemolytic activities of small molecules

Small molecule	MIC (μg/mL)			HC_{50} (μg/mL)
	S. aureus	*E. coli*	MRSA	
1a (n =2; R = $-C_{10}H_{21}$)	2	2	2	65
1b (n =4; R = $-C_{10}H_{21}$)	2	2	2	60
1c (n =6; R = $-C_{10}H_{21}$)	2	2	2	58
1d (n =8; R = $-C_{10}H_{21}$)	2	4	2	55
1e (n =10; R = $-C_{10}H_{21}$)	4	8	4	55
1f (n =12; R = $-C_{10}H_{21}$)	31	500	62	50
2a (n =6; R = $-C_8H_{17}$)	2	6	4	300
2b (n =8; R = $-C_8H_{17}$)	1	2	2	212
2c (n =2; R = $-C_8H_{17}$)	2	8	3.9	350
2d (n =4; R = $-C_8H_{17}$)	2	8	3.9	310
2e (n =10; R = $-C_8H_{17}$)	1	1	2	100
2f (n =12; R = $-C_8H_{17}$)	1	2	1	65
3a (n =10; R = $-C_6H_{13}$)	4	6	4	>1000
3b (n =12; R = $-C_6H_{13}$)	1	2	2	805
3c (n =2; R = $-C_6H_{13}$)	125	250	250	>1000
3d (n =4; R = $-C_6H_{13}$)	62.5	125	125	>1000
3e (n =6; R = $-C_6H_{13}$)	62.5	125	125	>1000
3f (n =8; R = $-C_6H_{13}$)	16	31	31	>1000

MIC = Minimum inhibitory concentration, MRSA = methicillin-resistant *S. aureus*

Table of Contents graphic